Sustainable Structures
ISSN: 2789-3111 (Print); ISSN: 2789-312X (Online)
http://www.sustain-dpl.com/journal/sust
DOI: 10.54113/j.sust.2026.000109

ORIGINAL ARTICLE

Eco-friendly protective coating made from geopolymer mortars for conventional concrete in a marine environment

Januarti Jaya Ekaputri[a,*], Chlarisya Eka Ningtyas[a], Iqlima Nuril Amini[b], Pitcha Jongvivatsakul[c], Tidarut Jirawattanasomkul[c], Himawan Tri Bayu Murti Petrus[d], Rita Irmawaty[e], Fakhruddin[e], Ari Widayanti[f], Retno Trimurtiningrum[g], and Yuya Takahashi[h]

[a]Department of Civil Engineering, Institut Teknologi Sepuluh Nopember, Surabaya 60111, Indonesia
[b]Department of Civil Engineering, State University of Surabaya 60232, Indonesia
[c]Center of Excellence in Innovative Construction Materials, Department of Civil Engineering, Faculty of Engineering, Chulalongkorn University, Bangkok 10330, Thailand
[d]Department of Chemical Engineering, Faculty of Engineering, Universitas Gadjah Mada, Yogyakarta 55284, Indonesia
[e]Department of Civil Engineering, Faculty of Engineering, Universitas Hasanuddin, Makassar 92171, Indonesia
[f]Transportation Study Program, Vocational Faculty, State University of Surabaya 60231, Indonesia
[g]Department of Civil Engineering, Universitas 17 Agustus 1945, Surabaya 60118, Indonesia
[h]Department of Civil Engineering, School of Engineering, The University of Tokyo, Bunkyo-ku, Tokyo 113-0033, Japan
[*]Corresponding Author: Januarti Jaya Ekaputri. Email: januarti@ce.its.ac.id

Abstract: Geopolymer mortar offers an eco-friendly way to protect concrete in harsh environments. Affordable materials such as fly ash (FA) and rice husk ash (RHA) improve sustainability, with RHA providing silica. The long-term effects of geopolymer and Portland cement in marine environments, especially under severe sulfate attack, remain largely unexplored. Understanding interface mineral formations is key to evaluating concrete's resistance to chemical infiltration. This study evaluated geopolymer mortar containing 0–10% RHA, replacing FA, as a protective layer for Portland concrete. Samples were exposed to chloride- and sulfate-rich seawater for 5 months to evaluate mechanical strength, porosity, sulfate resistance, chloride penetration, and interface behavior. A 5% RHA replacement (Si/Al = 3.26) optimized performance, enhancing chemical bonding at the interface through C-A-S-H formation. The geopolymer layer significantly improved sulfate resistance, outperforming Portland mortar with 20% FA (FPC). Marine exposure accelerated geopolymerization, increasing density and compressive strength while reducing chloride ingress. The protective N-A-S-H gel, stabilized by Fe, Al, and Mg, remained resistant to sulfate and chloride ions. Additionally, dissolved silica from RHA mitigated degradation and reduced CO_2 emissions by 62.1%. The study showed that geopolymer mortar is promising for jacketing, repairing, or patching concrete structures in marine environments.

Keywords: Fly ash, rice husk ash, geopolymer, wrapping material, seawater

1 Introduction

Developing infrastructure in coastal areas, such as bridges, piers, and tunnels, is essential for promoting economic growth. Concrete, as the most common material, is recognized for its durability compared to steel and is frequently used in marine construction. However, it faces significant challenges. Prolonged exposure to seawater with high chloride and sulfate concentrations can degrade concrete and reduce its service life. When chloride ions infiltrate the concrete, they react with cement hydration products, forming Friedel's salt and compromising the concrete's structural integrity [1]. The sulfate content and available alumina also contribute to the formation of ettringite and Friedel's salt. This

Received: 18 December 2025; Received in revised form: 4 July 2026; Accepted: 18 July 2026

generates expansive pressure, leading to cracks and reducing the concrete's performance [2]. Enhancing concrete's chloride-binding capacity is essential to address these challenges. This approach can reduce the concentration of free chloride ions, thereby delaying corrosion of steel reinforcement in reinforced concrete structures. Furthermore, sulfate attacks decalcify the $Ca(OH)_2$ and C-S-H phases, promoting the formation of gypsum and ettringite, which further weaken the concrete [3]. These challenges underscore the need for expertise in marine concrete construction, a field where knowledge and experience are valuable and essential.

Various studies proposed supplementary cementitious materials (SCM) such as fly ash (FA), rice husk ash (RHA), palm oil fuel ash, and blast furnace slag to enhance concrete durability by reducing pore connectivity [4–7]. Incorporating RHA particles decreases water absorption and sorptivity coefficient, while silica fume and RHA support the pozzolanic reaction, reducing $Ca(OH)_2$ content [8]. The pozzolanic reaction transforms $Ca(OH)_2$ into C-S-H, filling micro-pores and restricting chloride-ion penetration, thereby enhancing durability. However, using FA alone, even at 15% of the cement weight, can lead to corrosion of steel reinforcement after 4 years of seawater exposure, indicating the need for additional protective measures against chloride and sulfate attacks [9,10]. In several coastal bridges, reinforcement corrosion has been observed, primarily due to insufficient concrete cover. These concrete structures use 10–15% fly ash (FA) replacement. The reduced cover depth likely facilitated the penetration of aggressive agents, such as chlorides, from the marine environment, thereby accelerating corrosion despite the partial replacement of cement with FA.

Applying a protective coating effectively enhances concrete's resistance to chlorides. Epoxy-polyurethane and aliphatic acrylic coatings are most efficient in delaying corrosion initiation, especially in tidal zones [11]. The effectiveness of surface coatings in hindering chloride-ion diffusion in marine concrete has been demonstrated in relation to service-life predictions. A threshold depth of 50 mm and a target critical chloride concentration of 0.07% by weight of concrete have been established. Various surface treatments, including polyurethane, modified cementitious coating, and styrene acrylate, have been shown to enhance the longevity of concrete structures by 68%, 27%, and 11%, respectively. This evidence indicates that utilizing surface coatings for repairs significantly contributes to the durability of concrete when exposed to marine conditions [12, 13]. However, common coating materials have limited longevity and need periodic reapplication for sustained chloride resistance [14]. The efficacy of coatings is time-dependent, with the concentration of chloride ions impacting performance.

Recent research explores the development of concrete coating materials that are resilient to seawater exposure, with a focus on geopolymer materials. Geopolymer utilizes waste sources like FA, RHA, palm oil fuel ash, and sugarcane bagasse ash, reacting them with alkalis such as sodium silicate (Na_2SiO_3) and sodium hydroxide (NaOH). Fly ash-based geopolymers exhibit superior resistance to aggressive environments, attributed to a denser concrete matrix and smaller pore size [15]. Unlike Portland concrete, the sulfate and chloride attack mechanism on geopolymer concrete reveals the absence of binding between the ions and N-A-S-H [10, 16]. Chloride ions in geopolymer adhere physically to the surface of the N-A-S-H gel without reacting with the geopolymerization product [17]. Despite findings suggesting that sodium chloride (NaCl) and sodium sulfate (Na_2SO_4) can enhance the solubility and reactivity of fly ash, the mechanism of seawater attack on geopolymer materials in real environments remains insufficiently discussed.

Geopolymer paste and mortar, with low permeability, high bond strength, and good ductility [18], show promise as coatings for marine concrete structures [19]. Other aluminosilicate sources, such as metakaolin, ground granulated blast furnace slag, and silica fume, are often used for marine applications for corrosion resistance in aggressive environments [20]. Geopolymer, as an alkali-activated material with recommended precursors such as natural pozzolans, is a promising choice for coatings, retrofitted concrete repairs, rehabilitation, and sensing in different environments [12, 21, 22].

Geopolymers as structural elements offer benefits but are limited by their inherent brittleness, rapid setting time [23], and unpredictable long-term performance, which restrict their wider use. This brittleness leads to sudden failures under tensile and flexural stresses, and long-term stability concerns include shrinkage, microcracking, and aging-related phase changes. Additionally, studies on accelerated aging suggest potential crystallization and strength loss, raising durability concerns in different environmental conditions. These uncertainties hinder accurate performance predictions and complicate standardization efforts. Therefore, many studies suggest the use of fiber reinforcement and

nanomaterials to mitigate brittleness [24, 25]. The effectiveness of fibrous geopolymer varies based on fiber type, quantity, and matrix composition.

Despite the benefits and drawbacks of geopolymers, this material offers advantages in actual seawater environments due to its low calcium content. This characteristic enables it to resist deterioration resulting from calcium leaching triggered by barnacle invasions. Its stable chemical structure in seawater provides sustainable protection to Portland concrete (PC). In our previous study, a 40 mm geopolymer mortar coating significantly increased compressive strength from 37 MPa (28 days) to 52 MPa (90 days in seawater), preventing chloride ingress [26]. The denser microstructure at the geopolymer-PC concrete interface, which forms additional C-A-S-H products, distinguishes it from the PC interface area.

Enhancing the mechanical strength and durability of geopolymer involves adjusting the alkaline silica ratio or incorporating silica to reduce porosity [27]. Amran et al. [15] underscored the influence of Si/Al ratios on the structure of fly ash-based geopolymers. An abundant source of natural silica in Indonesia, Malaysia, Japan, and Thailand is RHA, which contains 91% silica due to the ability of plants to accumulate it from the soil [28–30]. As an example, in 2022, rice production in Indonesia was estimated at 55.67 million tons, with a quarter comprising rice husks [31]. There is significant potential for the use of RHA in geopolymer concrete. RHA decreases water permeability in geopolymer concrete, but higher RHA content as a precursor requires more alkali activators [32]. An ideal RHA content of up to 15% can help reduce permeability in ground granulated blast furnace slag (GGBFS)-based geopolymer concrete. It is essential to consider all these factors to achieve the desired permeability level. Adding up to 20% RHA to fly ash-based geopolymer concrete enhanced water resistance by promoting N-A-S-H gel formation and compacting the geopolymer structure [33]. The challenge of incorporating high volumes of rice husk ash (RHA) into geopolymer mixtures warrants further examination. Therefore, a research gap exists regarding the effectiveness of RHA in geopolymer mortars exposed to seawater, underscoring the need for further investigation of its performance in marine environments.

This study explores the use of RHA geopolymer concrete coating mortars with FA replacement levels ranging from 0% to 10% and examines their impact on workability. These 50 mm-thick mortars, coated on the inner concrete, were made from Portland concrete containing FA, mimicking the shield of existing structures. The concrete was immersed in the Madura Strait for 150 days, near industrial areas in Surabaya City, Indonesia, where it was subjected to severe sulfate conditions and chloride attack from seawater. The study analyzes chloride and sulfate binding in protective geopolymer mortars and compares them with pozzolan-based cement.

Geopolymer mortar exhibits strong adhesion to Portland cement surfaces, enhancing durability against sulfate attack and improving mechanical properties through the formation of C-A-S-H minerals. The geopolymerization process increases the mortar's density and compressive strength, especially with the addition of RHA, which shows significant strength improvements over 150 days. When exposed to seawater, RHA further enhances geopolymerization, resulting in higher compressive strength and reduced chloride-ion penetration and porosity. However, using more than 5% RHA, rather than fly ash, can reduce mortar strength due to increased porosity. Unlike traditional cement mortar, which increases in pH due to decalcification, geopolymer mortar maintains a lower pH and alters its mineral composition in response to ion attack. Overall, geopolymer mortar outperforms traditional cement mortar in strength and resilience against environmental challenges.

This study highlights the need for further research on RHA's effectiveness as a silica source for FA in geopolymer mortar exposed to seawater, suggesting a potential avenue for understanding geopolymer performance in marine environments. This approach aligns with circular economy principles by converting industrial byproducts into valuable resources and promoting resource efficiency in construction. Furthermore, this study suggests a potential area for further research to understand the performance of geopolymer materials in marine environments.

2 Materials and Methods

2.1 Materials

The materials utilized in this research include Portland Composite Cement (PCC) and fly ash (FA) sourced from Tanjung Jati B Power Plant, Indonesia. This coal-fired power plant is located on the northern seashore of Java Island, allowing the FA to contain chloride. Additionally, the materials consisted of RHA, river sand, and crushed stone with a maximum size of 10 mm. Observation of Fly Ash (FA) reveals small, spherical particles. Interestingly, within this particulate system, some spherical particles exhibit a unique structure in which they encapsulate several smaller microspheres. The employed FA contains 0.1% free chloride and 0.32% bound chloride. This value has been considered as the initial amount of chloride ions before the specimen was immersed in seawater. Fly ash (FA) comprises 54.31% silica, yet only 64% of this silica is soluble, with a significant portion being partially reactive. This is a typical phenomenon of using FA as the main precursor [34]. The fineness of fly ash (FA) was assessed by determining the percentage of particles 87.5% passing through a No. 325 (45 µm) sieve, as specified by ASTM C618 [35]. The RHA particles are porous and flake-like. Particles of FA and RHA analyzed with scanning electron microscopy (SEM) are shown in **Fig. 1** The chemical composition of both FA and RHA is listed in **Table 1**.

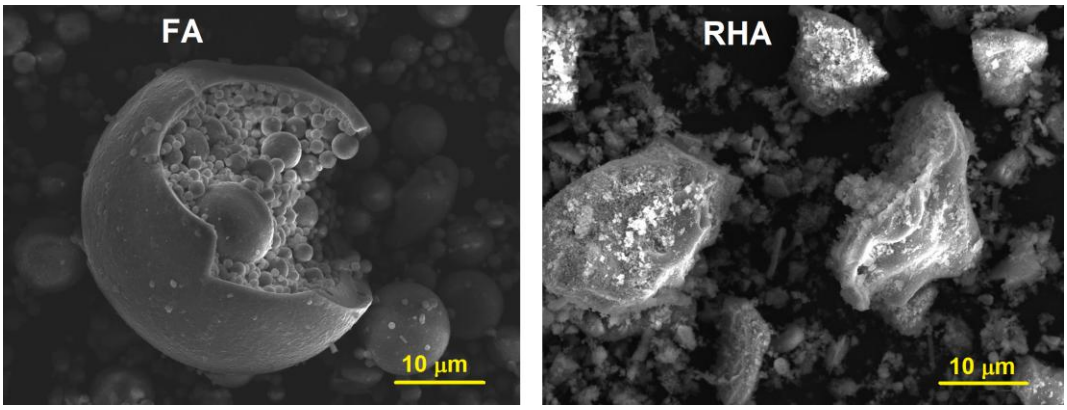

Fig. 1. SEM analysis at 2000× magnification.

Table 1. Chemical composition of FA and RHA (% by mass)

Material	Oxides (%)									
	SiO_2	Al_2O_3	Fe_2O_3	CaO	MgO	Na_2O	K_2O	P_2O_3	SO_3	LOI
FA	54.31	17.62	10.14	5.62	2.98	3.57	1.6	0.36	0.86	2.19
RHA	92.04	0.89	0.49	0.80	0.78	0.06	2.48	1.4	0.64	0.18

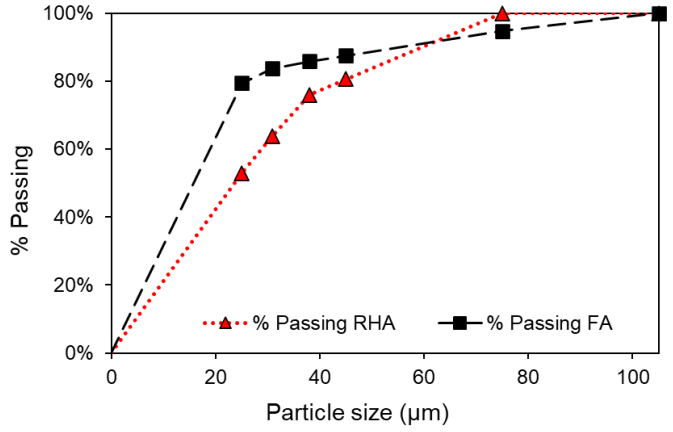

Fig. 2. Particle size analysis with wet sieving

To enhance the reactivity of the geopolymer matrix, rice husk ash (RHA) was incorporated as a key supplementary silica source, thereby improving the overall strength and durability of the final product. The RHA underwent combustion at 500ºC for 10 hours, and subsequently, 80.6 of % particles passed through sieve no. 325 (45µm). It was found that the amorphous phase of RHA constitutes 74%, comprising amorphous silica minerals, predominantly quartz and cristobalite. RHA is coarser than FA, as illustrated in **Fig. 2**. In the same alkaline mixture, a precursor with higher RHA may show a delay

in compressive strength development.

2.2 Preparation and Selection of Mortar Mixture

Studies recommend incorporating ground granulated blast-furnace slag (GGBFS) into marine geopolymers to enhance sulfate resistance. [36]. GGBFS was excluded from this study because it reduces workability and speeds up setting time.

Fig. 3 Flow table tests for mortar.

Fig. 3 illustrates the experiment from the mortar workability tests conducted with a flow table, which followed the standards in ASTM C1437 − 20 [37]. The images, arranged from left to right, depict mortar samples with RHA percentages of 0%, 2.5%, 5%, 10%, and 15%. The furthest image on the right shows mortar made with Portland cement. The results indicate that the inclusion of rice husk ash (RHA) negatively impacts the mixture's workability. In particular, incorporating 15% RHA with fly ash resulted in insufficient mortar fluidity, preventing proper filling of the mold for IC concrete. Consequently, the maximum allowable RHA content was restricted to 10%.

2.3 Preparation of Inner Specimens and the Coating Method

The test used 50 mm-diameter, 100 mm-tall IC (inner concrete) cylinders as specimens. Since the seawater exposure period was under 5 months, rebar is not discussed in this paper. A diagram illustrating a way to encapsulate the IC test sample blocks with mortar is given in **Fig. 4**. There is a rationale for our choice of a mortar thickness of 5 cm. The incorporation of chloride thickness enhances the compressive strength of concrete. The high binding capacity of the coating material has effectively reduced free chloride levels. According to ACI PRC-357 [38], the minimum recommended concrete cover over primary reinforcement for structures located in waterfront and coastal marine environments is 7.5 cm.

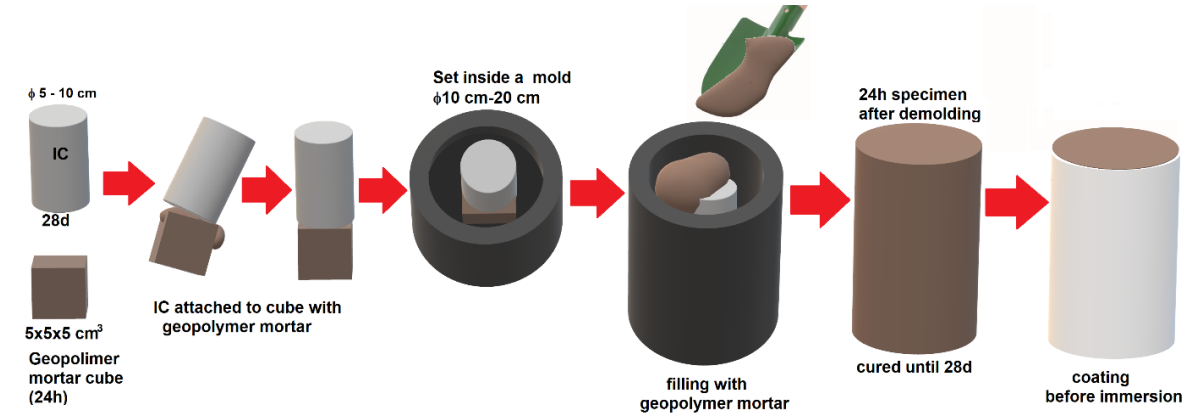

Fig. 4. Encasing inner concrete (IC) with mortar.

Our prior research conducted in submerged zones and with corrosion precipitation [26,39] indicated that at depths between 2.5 and 4 cm, the free chloride content within the concrete was below 0.15%, which meets acceptable limits for reinforced concrete's chloride concentration. The suggested maximum coating thickness is 4-5 cm. Furthermore, increasing cover depth by 10 mm yields roughly an 8% to 10% improvement in service life; similarly, raising it by just 5 mm can extend service life by about 4% to 5%. Although changes in concrete cover depth have a comparatively modest impact on residual service life compared with other factors, ensuring optimal coverage remains crucial for effective design. Sufficient cover depth serves as vital protection against ion infiltration and helps postpone corrosion initiation [40].

Although the specimens were subjected to elevated sulfate concentrations in an aggressive environment, the exposure duration was limited. Consequently, the effects of corrosion on the rebar are

not examined in this study. For extended periods (ranging from 6 months to 2 years or more), it is essential to consider the influence of biofilms and barnacles. The development of microfouling, primarily microbial biofilms, is influenced by marine environmental conditions, substrate characteristics, and immersion time. Some studies have indicated that marine organisms such as barnacles and oysters that adhere to concrete surfaces create protective layers, which can slow down chloride ion diffusion [41]. Conversely, other research has determined that microbial biofilms in marine environments significantly impact concrete substrates by initiating and hastening biodeterioration through various biochemical processes [42].

2.4 Submerged Zone Exposure

The total chloride and total sulfate levels in the seawater at the immersion location, as observed over the past eleven years, are illustrated in **Fig. 5**.

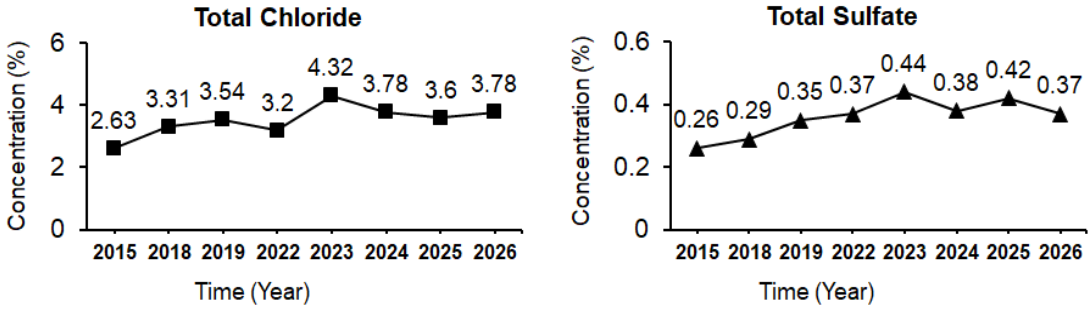

(a) Chloride (b) Sulfate

Fig. 5. An increase in the concentration of (a) chloride and (b) sulfate in the Madura Strait.

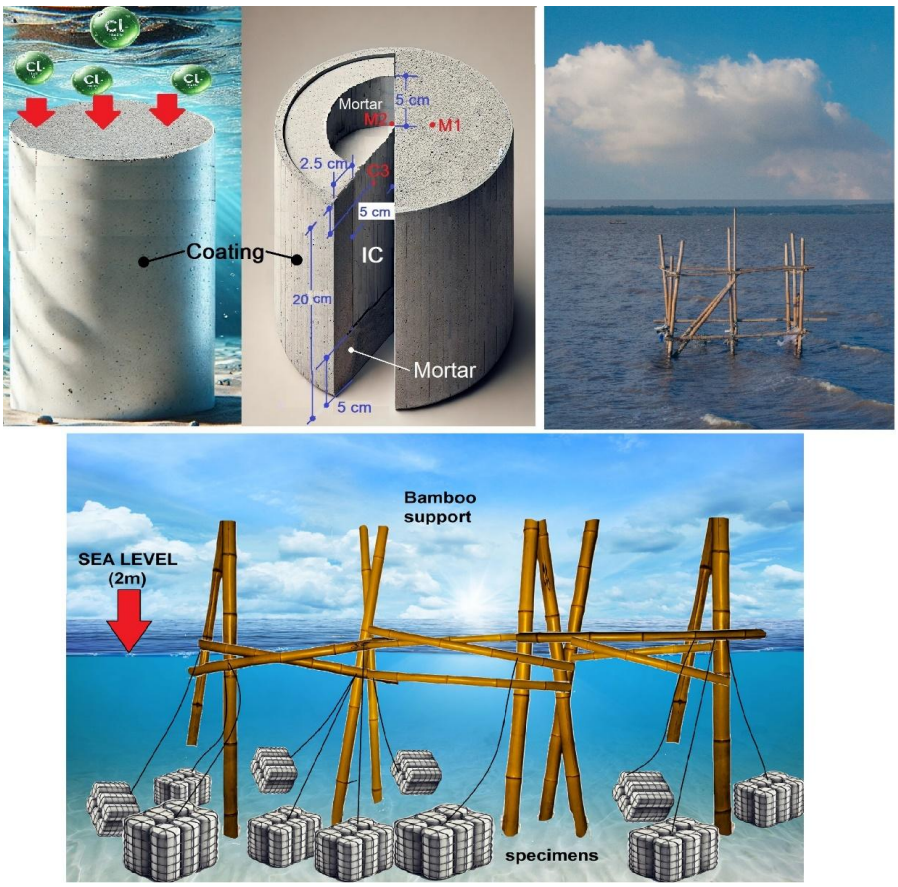

Fig. 6. Specimen details and submerging scheme.

The sulfate content in the Madura Strait has also increased continuously since 2015. According to the ACI 318-19 standards [43], the sulfate exposure in the strait falls into the severe category (S2). Unlike typical laboratory-scale simulations that focus solely on the effects of chloride using salt

solutions, real marine environments involve multiple factors such as temperature fluctuations, sulfate-chloride interactions, and various other seawater constituents. These additional factors significantly influence the durability of concrete and must be accounted for when assessing the performance of mortar-coated concrete in marine environments.

All specimens were immersed in the submerged zone in the Madura Strait for five months following a seawater exposure scheme (**Fig. 6**). Before immersion, the sides of the specimens were coated with a 5-cm-thick resin layer (Sikagard 63N) to prevent seawater penetration. The top and bottom were exposed to seawater. Bubble wrap protected the specimens from colliding during immersion. The mortar cover thickness was 5 cm, as recommended by previous studies [26,44]. Three observation points (M1, M2, C3) were used to analyze pH, chloride, and sulfate ions. At 28 days, the IC was wrapped in geopolymer mortar to form a composite and underwent moist curing for another 28 days before seawater immersion at 0, 30, 60, 90, 120, and 150 days.

The curing process is essential for achieving the required strength and durability of concrete and mortar. However, environmental conditions during curing greatly affect material quality, especially strength development and long-term performance. As a component of an initial investigation, we analyzed four distinct materials: (1) geopolymer mortar (GN), (2) Portland cement concrete integrated with 20% fly ash (FA) to produce the IC (FPN), (3) geopolymer mortar synthesized with alkali and seawater, aged 28 days before immersion (GS-28), and (4) geopolymer mortar formulated with alkali and seawater, aged 1 day before immersion (GS-1). These materials were subjected to a variety of curing environments, encompassing freshwater, saltwater, and seawater. Cylindrical specimens, characterized by a diameter of 10 cm and a height of 20 cm, were fabricated for the assessment of compressive strength. The findings after 90 days are presented in **Fig. 7**.

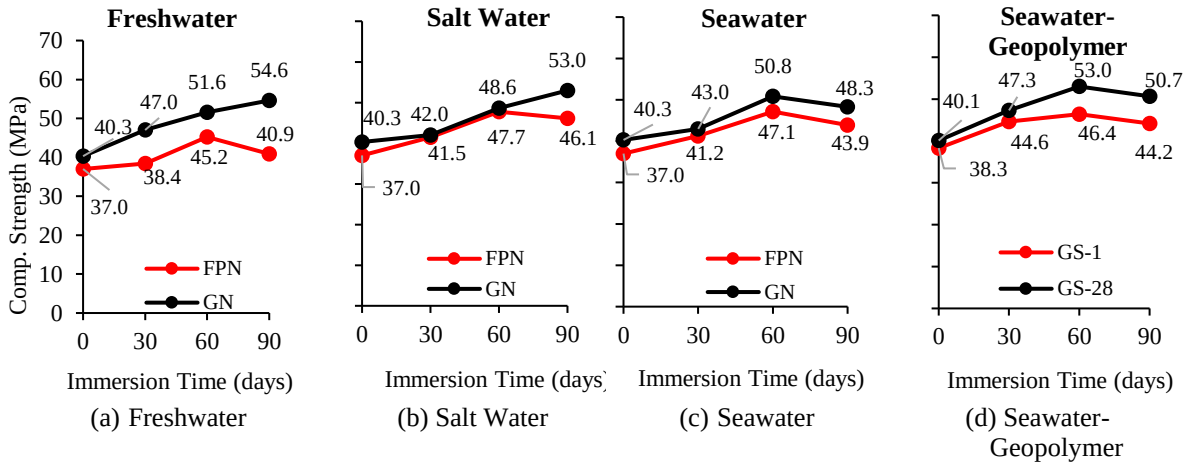

Fig. 7. Strength of geopolymer (GN) mortar made with water, made with seawater (GS), and Portland concrete (FPN) with different curing conditions.

Research on the negative effects of long-term curing in freshwater on concrete strength is limited. Curing is generally recognized for enhancing strength by facilitating continued hydration. However, certain studies have indicated that extended curing durations may not always lead to increased strength and, in some cases, could contribute to strength reduction and decreased durability of concrete [45,46]. Preliminary investigation data indicated that geopolymer (GN) exhibits greater long-term resistance to curing in both freshwater and saltwater than Portland concrete (FPN). However, prolonged exposure to seawater, particularly for more than 90 days, significantly reduces the mechanical strength of both materials, underscoring the aggressive nature of the marine environment on GN, FPN, and GS. It is noteworthy that exposure to seawater did not substantially affect the mechanical properties of geopolymer mortar (GS), unlike in Portland cement concrete. This observation inspired the current investigation, suggesting that geopolymer-based mortar may serve effectively as a protective encasement for existing constructions against the deleterious effects of seawater.

Sea sand and seawater, rich in chloride and sulfate ions, influence the properties of geopolymer concrete. Chloride ions had a minimal impact on compressive strength because the dense FA matrix resisted penetration. Seawater curing increased strength by up to 15%, preventing reactant leaching and stabilizing the structure [47]. Although chloride disrupted internal polymerization, it formed a protective

surface layer, improving durability and highlighting seawater's potential when used with optimized molarity and curing methods [48].

In this study, the IC was prepared and subjected to a 28-day moist-curing period. Subsequently, coating mortars were applied for IC using the composition specified in **Table 2**.

Table 2. Concrete composition (kg/m³)

Code	FA	RHA	PCC	Fine Aggregate	Water	Na_2SiO_3	NaOH 10 M	Si/Al
IC	92	-	371	872	218	-	-	-
GN	847	-	-	990	-	242	121	3.02
G2.5	825	18	-	990	-	242	121	3.14
G5	804	36	-	990	-	242	121	3.26
G10	762	72	-	990	-	242	121	3.54
FPC	111	-	444	1528	250	-	-	-

In the IC mixture, FA was used to replace 20% of the Portland cement composite (PCC) weight at a water-to-binder ratio of 47%, yielding a compressive strength of 37 MPa at 28 days. The strength met the specific requirements outlined in ACI 318M-19 [43], for concrete designated for use in chloride environments, which mandates a minimum compressive strength of 35 MPa.

While this composition satisfied the minimum requirements, it fell short of the maximum water-to-binder (*w*/*b*) ratio limit of 40% stipulated by the standard. Moreover, the water content in the mixture exceeds 200 kg/m^3, increasing the risk of chloride and sulfate ions penetrating. This specific design mix was deliberately selected to assess the vulnerability of concrete in a seawater environment. The geopolymer mortar used sodium silicate (Na_2SiO_3) and 10 M sodium hydroxide (NaOH) as alkali activators, with an Na_2SiO_3-to-NaOH ratio of 2. The FA to alkali activator ratio was 70:30, and the binder to fine aggregate ratio was 55:45. RHA replaced FA at volumes of 0%, 2.5%, 5%, and 10%, denoted as GN, G2.5, G5, and G10, respectively. The Si/Al molar ratio in the geopolymer mortars was determined using silicon sources from FA, RHA, and Na_2SiO_3, with the sole aluminum source from FA. After wrapping, all specimens underwent an additional 28 days of moist curing before being ready for resin coating and seawater immersion. Except for G10, which achieved a strength of 25 MPa, the remaining mortars demonstrated a 28-day compressive strength within the 40-41 MPa range. We prepared the Portland-based control mortar (FPC) for reference. Mortar specimens used for this compressive strength test were cylindrical mortars 5 cm in diameter and 10 cm in height.

2.5 Test Procedure for pH, Chloride Ion, Porosity, and Sulfate Penetration

The tests included compressive strength, free and bound chloride content, total sulfate content, pH value, and porosity. Specimens were immersed in seawater for 0, 30, 60, 90, 120, and 150 days. **Fig. 8** shows the specimen surface after immersion before testing; from left to right are GN, G2.5, G5, G10, and FPC, respectively. The top image shows the test specimen's surface after 1 month of immersion, while the bottom image shows the surface after 150 days of immersion. All barnacles on the surface were removed before sampling at point M1.

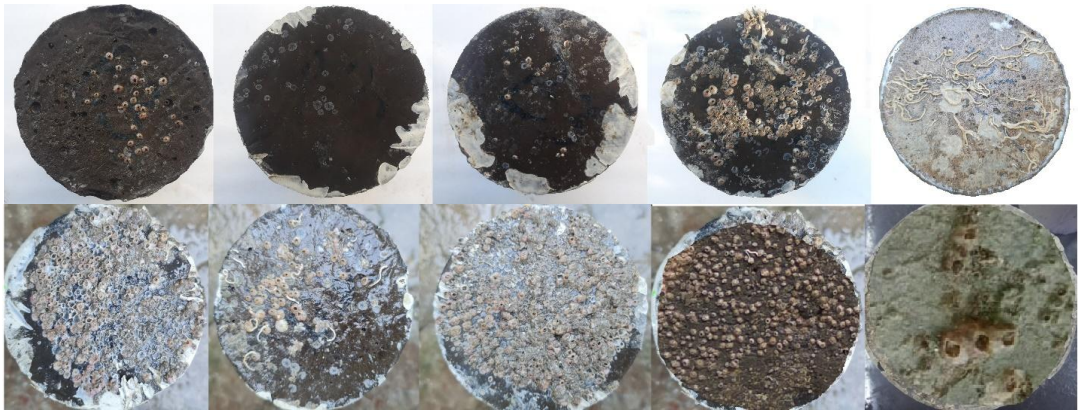

Fig. 8. Specimen surface after 30 days of immersion (top) and 150 days of immersion (bottom).

2.5.1 Compressive Strength of Concrete Specimens Encased in Mortar

The specimens were made into composite materials, with IC enclosed in wrapping mortars. This study aimed to assess the compressive strength of the composites before and after seawater immersion. Initial tests were conducted using a hydraulic testing machine, followed by subsequent tests after seawater exposure. Each variation included four identical specimens, and the average compressive strength was calculated. The tests were conducted at the Concrete, Advanced Materials, and Mechanical Computing Laboratory at ITS, Surabaya, Indonesia. The compressive strength (σ) was determined using Eq. (1), where strength equals the force (P) applied to the concrete surface divided by the surface area (A). ANOVA was used to analyze the effects of RHA substitution, soaking time, and their interaction on strength.

$$\sigma = P / A \tag{1}$$

2.5.2 Chloride Content, Sulfate Content, Carbonation, and pH

At seawater immersion intervals of 30, 60, 90, 120, and 150 days, chloride penetration test assessments of the mortar were conducted using the argentometry method. To assess the effectiveness of wrapping mortar, mortar samples were extracted only from the surface (M1) and at 4.9-5.0 cm from the surface (M2) to determine free chloride, bound chloride, sulfate, and pH levels. In this study, the chloride ingress profile in concrete is not fully explained. Therefore, chloride penetration in mortar layers is not presented. At points M1, M2, and C3, pH, chloride, carbonation, and sulfate analyses were conducted for each sample, and the 2 test results were averaged. After reaching the appropriate age, the mortar surface, including adhering barnacles, was cleaned, and the resin coating was removed. For M1, the surface exposed to seawater was ground to a depth of 2 mm for sampling. Mortar slabs were cut at a distance of 4.8 cm from the surface and ground to a depth of 1-2 mm to obtain samples representing point M2. At point C3, where the depth from the surface is 6.9-7.1 cm, the sample was cut and ground. Sulfate content was measured using spectrophotometry. The carbonate ion (carbonate and bicarbonate) content was measured by acidimetric titration. The preparation process for mortar samples designated for the durability test is illustrated in **Fig. 6**. The chloride content is typically determined in the sample as parts per million (ppm). For mortar or concrete samples, it is necessary to convert these values to the binder weight for a more meaningful assessment. The conversion of chloride content from parts per million (ppm) to a percentage of the weight of the binder was calculated using Eq. (2).

$$C = \frac{p \times W_{\mathrm{m}}}{\sigma} \times 10^{-6} \times 100\% \tag{2}$$

where C represents the percentage of chloride concentration to the weight of the binder, p is the concentration of chloride ions in the mortar in ppm, W_{m} is the dry weight of the mortar (kg), and W_{b} is the weight of the dry binder (kg).

2.5.3 Porosity Test

Porosity testing adheres to the guidelines outlined in ASTM C642-13 [49], standards for the mortars in point M2. The test results yielded the open-pore volume. Calculation of the total pore volume involved grinding the sample and measuring its volume, accounting for both open and closed pore volumes, formulated in Eq. (3) to Eq. (5). The total pore volume is subsequently interpreted as the combined sum of the open pore volume and the closed pore volume, where g_1 is the bulk density in dry condition (g/m³), g_2 is the apparent density (g/m³), and g_3 is the absolute density (g/m³).

$$Open\ porosity = \left[\frac{g_2 - g_1}{g_2}\right] \times 100\% \tag{3}$$

$$Total\ porosity = \left[\frac{g_3 - g_1}{g_3}\right] \times 100\% \tag{4}$$

$$Closed\ \ porosity = Total\ \ porosity - Open\ \ porosity \tag{5}$$

2.5.4 Microstructure Analysis

Scanning Electron Microscopy (SEM) and X-ray Diffraction (XRD) analysis were conducted to investigate matrix alterations in the wrapping mortar following immersion in seawater. SEM analysis

was performed with a JEOL JSM-6510-A. The crystal structure content analysis was conducted using an X-ray Diffractometer (XRD) X'Pert MPD with Kα and λ radiation of 1.5406 Angstroms.

3 Results and Discussion

3.1 Compressive Strength

Fig. 9 presents the compressive strength test results for composite concrete specimens in which IC is encased in mortar, before and after seawater immersion for 30 to 150 days. At 28 days (0 days soaking), adding 5% RHA increased the geopolymer mortar's compressive strength from 40.3 MPa (GN) to 45.1 MPa (G5), attributed to silica particles from RHA creating a denser matrix. This micro silica-filler effect enhanced the strength of the G5 specimen. However, incorporating 10% RHA (G10) significantly reduced the initial strength to 26.9 MPa. This phenomenon aligns with Mehta et al. [50], who reported that using more than 15% RHA hinders geopolymerization, reducing strength. The low alumina content in RHA increased the Si/Al ratio from 3.02 (GN) to 3.54 (G10), thereby decreasing strength, as it deviates from the optimal range of 1.875 to 2.078, as noted by Wijaya et al. [51]. The lack of alumina in RHA contributes less to strength development compared to FA, while the high silica content slows the reaction, requiring more time to achieve optimal strength [52].

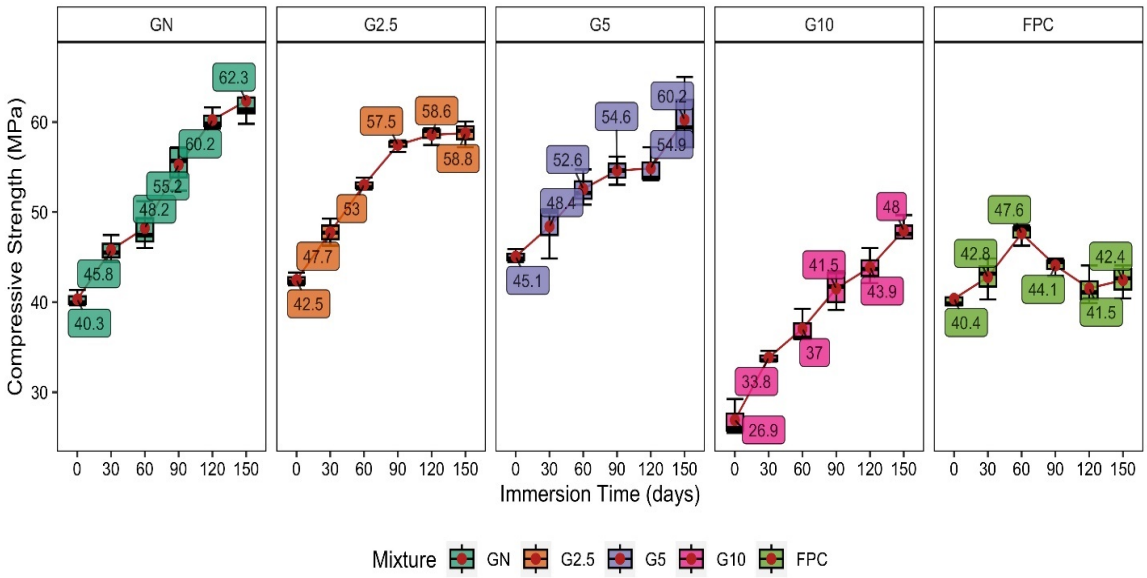

Fig. 9. Strength of wrapped concrete during submersion.

Extended seawater exposure for 150 days effectively preserved the compressive strength of the composite of IC encased in geopolymer mortar. All specimens showed consistent strength gains ranging from 33% to 78%. The G10 mortar demonstrated the highest increase, rising 78% from 26.9 MPa to 48 MPa after 150 days, surpassing FPC strength after 120 days. The initially lower strength of high Si/Al ratio systems is attributed to slower polycondensation, driven by the more challenging dissolution of silica compared to alumina. This slower reaction prolongs the time needed to reach peak strength. Other studies report that beyond 10 %, compressive strength decreases to a level lower than the reference strength (0 % RHA) [53]. The ongoing geopolymerization, driven by unreacted FA and RHA, continues to enhance strength even at 365 days [54]. The compressive strength of FA-based geopolymers depends on the LOI, precursor fineness, silica solubility, and the Si/Al ratio in the mixture [55]. The best compressive strength is achieved at a specific Si-to-Al ratio [56]. A higher silica content will decrease compressive strength. However, in corrosive environments such as seawater, a higher silica content is necessary for durability. This is the reason this study uses a minimum ratio of 3.0. In G10, despite its high silica content due to RHA, the RHA fineness is lower than that of FA, resulting in lower solubility. This hinders the increase in compressive strength in the early stages.

The primary purpose of incorporating rice husk ash (RHA) is to enhance durability, as the mortar serves as a protective coating rather than a load-bearing material. Despite some studies indicating that RHA may reduce compressive strength, composite specimens have shown increasing strength over 150

days of immersion. RHA's main function is to resist chloride and sulfate attacks in seawater and prevent early-age penetration, as confirmed by chloride content tests demonstrating reduced chloride ingress. Furthermore, RHA provides reactive silica, which promotes the formation of a stable N-A-S-H structure in geopolymers, thereby enhancing resistance to chloride penetration.

In contrast, FPC mortar showed a 17% increase in compressive strength after 90 days of immersion, followed by a 12.5% decrease at 150 days. The strength gain was due to pozzolanic reactions, which densified the mortar [57]. However, the subsequent decline was caused by chloride- and sulfate-induced degradation of C-S-H minerals, leading to the formation of M-S-H, brucite, gypsum, and ettringite, and resulting in cracks and reduced mechanical strength [2,10,58,59]. In comparison, advanced geopolymerization and pozzolanic reactions in the geopolymer mortar significantly enhanced its microstructure and compressive strength.

3.2 Analysis of variance for compression strength

An analysis of variance (ANOVA) was performed to evaluate the effects of RHA substitution, immersion time, and their interaction on compressive strength as the dependent variable. **Table 3** presents the ANOVA results at a 95% confidence level. The analysis confirmed that RHA substitution, immersion time, and their interaction significantly affected compressive strength (P = 0.000, below the $\alpha = 0.05$ threshold).

Table 3. Results of ANOVA analysis for compressive strength test

Source	DF	Adj SS	Adj MS	F-Value	P-Value
RHA (%)	3	3057.00	1018.98	258.13	0.000
Immersion time (days)	5	3240.90	648.19	164.20	0.000
RHA (%)*Immersion time (days)	15	207.80	13.86	3.51	0.000
Error	56	221.10	3.95		
Total	79	6611.40			

ANOVA (Analysis of Variance) evaluates whether independent variables, or factors, exert a statistically significant effect on the dependent variable, also known as the response. However, ANOVA does not identify which specific treatments result in distinct responses. To address this, ANOVA is often complemented by post hoc pairwise comparisons. Factorial plots are used to plot the relationships between responses and variables, as presented in **Fig. 10**.

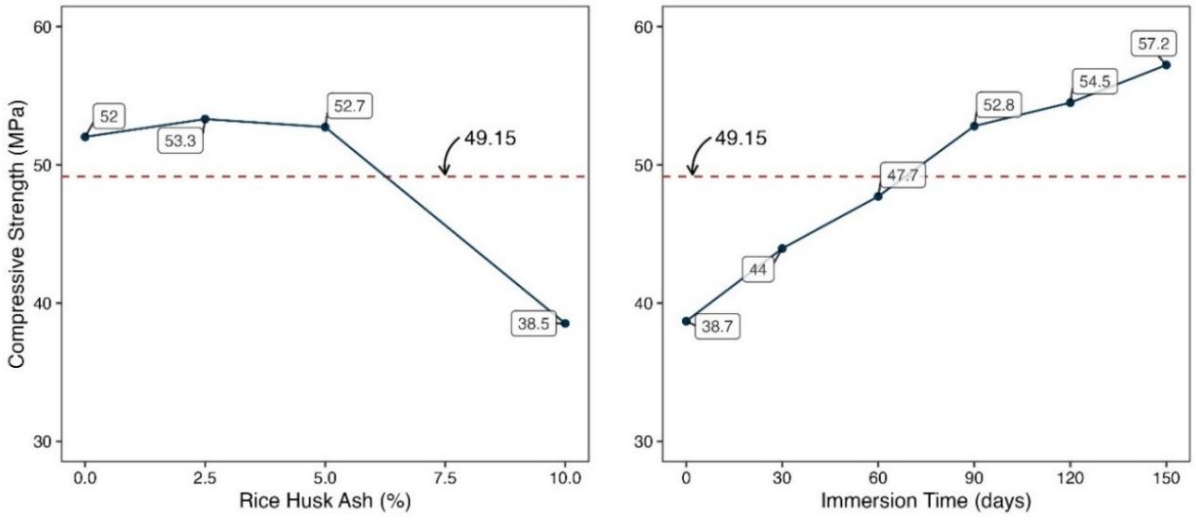

Fig. 10. The relation between RHA substitution and immersion time on the compressive strength test.

A post hoc Tukey's test was conducted to discern variations in treatment responses. The resulting grouping information displays significant and non-significant differences among treatments. Groups that do not share a letter differ significantly.

Table 4 provides details on the treatment comparison of RHA in concrete, revealing that the 0%, 2.5%, and 5% RHA treatments share a letter, indicating no significant difference in response. Conversely, the 10% RHA treatment is significantly different from all other treatments, as indicated by

the absence of shared letters.

Table 4. Grouping information using the Tukey Method and 95% confidence (effect of RHA)

RHA (%)	N	Mean	Grouping
2.5	19	53.309	A
5.0	20	52.730	A
0.0	20	52.024	A
10.0	21	38.529	B

Table 5 presents a comparison of treatment effects by immersion time. The results indicated that the treatments with 90 and 120 days of immersion time share a letter, implying a non-significant difference in response. Conversely, the treatments with 0, 30, 60, and 150 days of immersion time do not share a letter, indicating a significant difference.

Table 5. Grouping information using the Tukey Method and 95% confidence (effect of immersion time)

Immersion time (days)	N	Mean	Grouping				
150	16	57.225	A				
120	13	54.498		B			
90	15	52.805		B			
60	12	47.721			C		
30	12	43.951				D	
0	12	38.691					E

3.3 Interface Between Geopolymer-Concrete

Fig. 11 shows the specimen damage after the compressive strength test. The geopolymer mortar remained strongly adhered to the concrete surface, while the FPC mortar peeled off completely. Geopolymer mortar bonds to concrete better than FPC mortar, confirming its superior strength and shear performance as a repair material for Portland concrete [60,61].

This indicates that the bond between geopolymer mortar and concrete is stronger than that between FPC mortar and concrete. These results, consistent with previous studies, confirm the superior bond strength and shear capability of geopolymer materials when used as repair materials for Portland concrete [60,61].

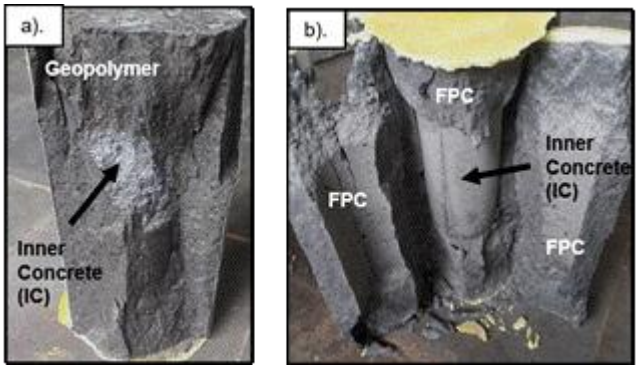

Fig. 11. Bond between: (a) geopolymer mortar-concrete and (b) FPC mortar-concrete.

Fig. 12 illustrates the interface layer between GN mortar and the inner concrete, showing a distinct 0.47 mm-thick transition layer that highlights the interface's compactness. The image, captured with a Dino-Lite Premier Digital Microscope AM4113/AD4113, shows that the geopolymer mixture can infiltrate the open pores of the concrete surface, forming a new layer. Elemental mapping revealed the distribution of essential elements at the composite's interface layer. EDS with SEM enabled precise elemental analysis. The region's distinct elemental composition indicates that the interface is heterogeneous. These maps reveal complex interactions between the geopolymer layer and nearby Portland concrete.

Fig. 13 displays the mapping, revealing distinct patterns in the distribution of Calcium (Ca), Silicon (Si), Aluminum (Al), and Sodium (Na), shedding light on their roles in interfacial bonding. SEM analysis shows a strong connection between the geopolymer and interface layers. N-A-S-H forms in the

mortar, while C-A-S-H attaches to the geopolymer gel and fills gaps with hydration products. Elemental analysis at a selected point shows mass ratios of 21.0% Calcium (Ca), 8.3% Silicon (Si), and 1.7% Aluminum (Al), providing insights into the structural characteristics and elemental composition at the interface. The gradual color change at the geopolymer-cement paste interface indicates a reaction between the geopolymer matrix and cement. The robust adhesion and uniform structure at the geopolymer-inner concrete (IC) interface result from the formation of C-A-S-H gel. The content of Ca, Si, and Al at the interface is crucial. The placement of geopolymer mortar over IC with available $Ca(OH)_2$ triggers a reaction between calcium from $Ca(OH)_2$ and SiO_2 and Al_2O_3 from FA, leading to C-A-S-H formation.

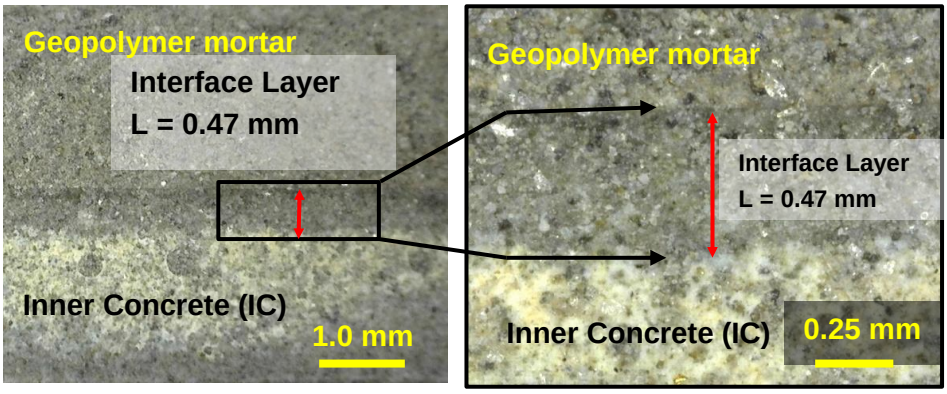

Fig. 12. Interface layer with a magnification of 40× (left) and 223× (right).

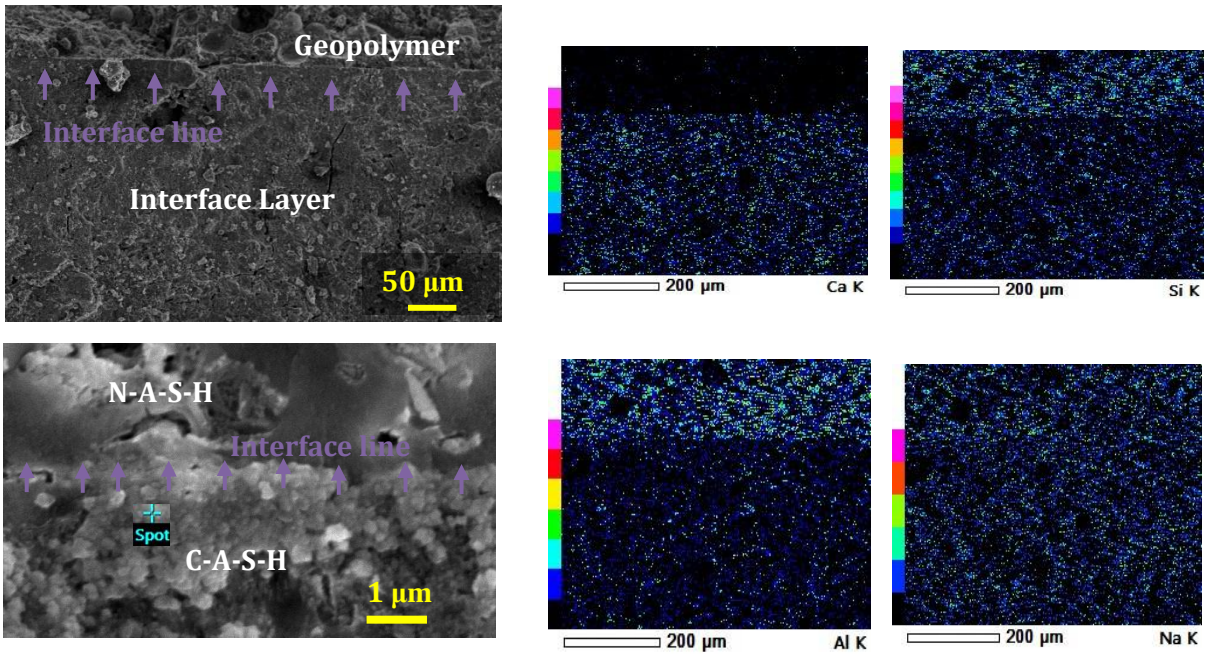

Fig. 13. Elemental mapping of the interface layer.

The XRD test results for the interface area between the geopolymer mortar and concrete at the age of 7 days are presented in **Fig. 14**. The presence of the C-A-S-H phase is detected. On the concrete side (IC), mineral cement hydration products, such as C-S-H and $Ca(OH)_2$ (marked in red), are observed. Unreacted cement product is represented by calcite. Meanwhile, on the geopolymer mortar side, geopolymerization products marked in blue, including the N-A-S-H and N-A-S phases, are identified alongside unreacted FA products represented by quartz, magnetite, and diopside.

In the geopolymer mortar, FA is activated by an alkali solution, forming $Si(OH)_4^-$ and $Al(OH)_4^-$ monomers. This activation promotes the formation of C-A-S-H in the interface layer through reactions between $Ca(OH)_2$ from the IC surface and the alumina and reactive silica in the mortar. However, low-calcium FAs exhibit limited reactivity, often requiring over 28 days for C-A-S-H formation via the pozzolanic reaction [62,63]. The formation of C-A-S-H gel strengthens the bond between the geopolymer mortar and concrete, filling any gaps and creating a dense interlayer that enhances

resistance to aggressive ion attacks [64]. This C-A-S-H layer offers exceptional protection against sulfate ions, a key factor in concrete durability [65,66]. By improving both mechanical properties and chemical resistance, geopolymer coatings can significantly extend the service life of concrete structures. While low-calcium FA forms C-A-S-H, high-calcium FA often produces C-N-A-S-H gel [67]. The chemical bond between aluminosilicate materials and sodium silicate in the geopolymer layer reinforces the adhesion to the concrete surface [68].

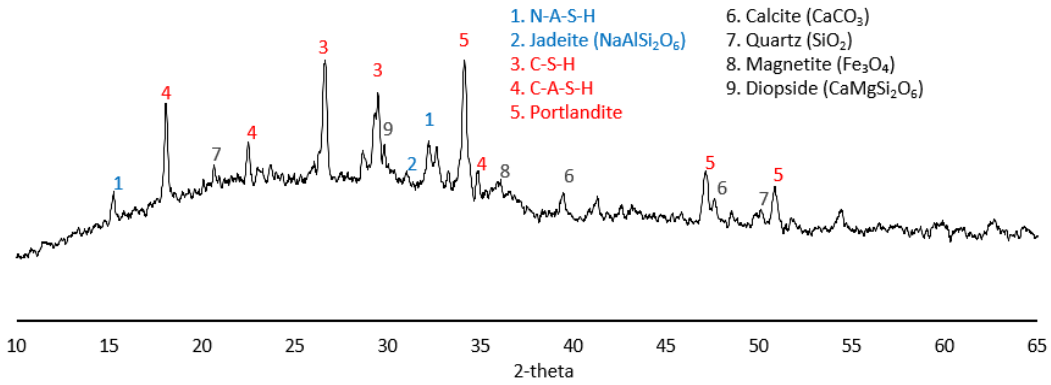

Fig. 14. Minerals in the interface layer of geopolymer mortar and concrete at 7 days.

3.4 Pore Characteristics of Wrapping Mortar

This study analyses two types of pores: open (permeable) and closed (impermeable). **Fig. 15** presents the porosity test results, including open, closed, and total porosity, for all variations at 0, 30, 60, 90, 120, and 150 days of immersion. Open pores are permeable, allowing air or water penetration, while closed pores are impermeable and withstand hydrostatic pressure, indicating concrete's tightness. Open pores contribute to porosity and reduce durability by facilitating chloride ion absorption. The results show that incorporating up to 5% RHA (G2.5 and G5) reduces open porosity. This reduction is due to silica particles from RHA filling micropores and microcracks with secondary C-S-H gel, mitigating cracks caused by crystallization and shrinkage stress.

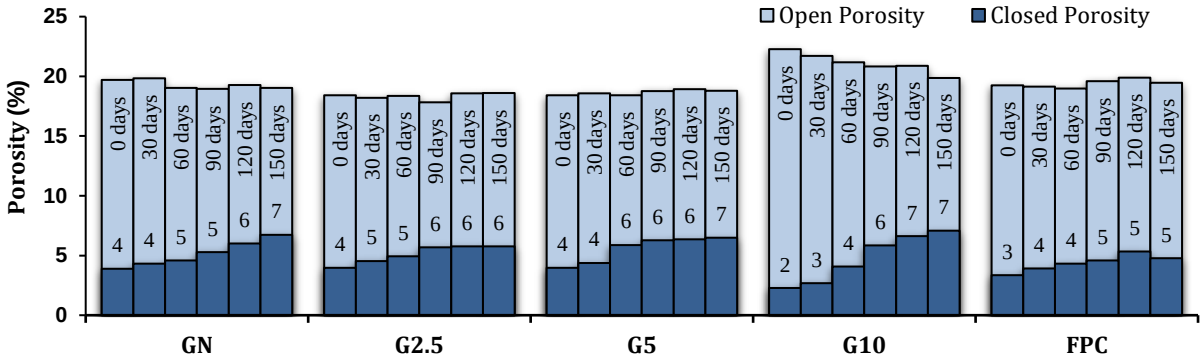

Fig. 15. Porosity of mortars during submersion.

The denser pore structure contributed to the increased compressive strength in G2.5 and G5 mortars at 28 days (before immersion). However, at 10% RHA content (G10), open porosity increased significantly, resulting in a reduction in strength. SEM analysis at 2000× magnification in **Fig. 16** shows that the N-A-S-H gel in G5 at 28d is the densest. Similar trends of increased porosity at RHA levels above 10% have been reported, attributed to the porous nature of RHA, which forms clusters of pores and cracks in the geopolymer matrix [33,69].

During immersion, all geopolymer mortars developed more closed pores, raising density as chemical reactions reduced pore size. Although seawater exposure could induce hydrolytic reactions, the Na cations in seawater mitigated cation leaching from the geopolymer mortar. Unreacted fly ash and silica particles from RHA continued to react, further densifying the gel. The solidified system also prevented dealumination, avoiding gel dissolution and strength loss. Observations suggest that available cations in the soaking water support continuous geopolymerization throughout the immersion period [16,70]. The most significant increase in density was observed in the G10 specimen, which had the

highest Si/Al ratio of 3.55. This rise in density corresponded to a remarkable increase in later strength. The inclusion of rice husk ash (RHA) reduced capillary pore volume while increasing gel pores, due to the silica-filling effect within the 3D geopolymer framework and to increased N-A-S-H gel formation. However, the lower polycondensation rate of silica compared to alumina-silica particles prolonged the densification process. Geopolymer systems with a high Si/Al ratio (>2) form polysialate-disiloxo or polysialate-multisiloxo structures, contributing to a denser and more homogeneous matrix [71].

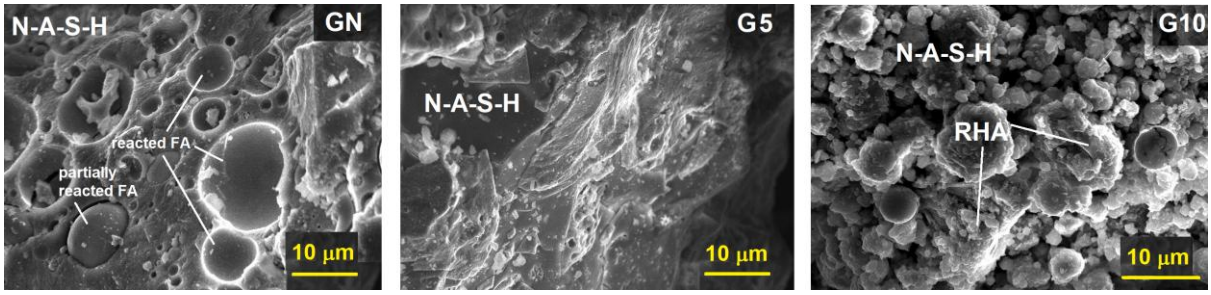

Fig. 16. SEM analysis for GN, G5, and G10 before immersion

The FPC mortar showed increased closed porosity, indicating a pozzolanic reaction from FA activation. The density rise was attributed to gypsum and salt formation due to seawater infiltration. Although compressive strength increased by 17% at 60 days, it decreased by 12.5% at 150 days, likely due to expansive pressure from aggressive ions accumulating in the pores, weakening the concrete. Pore size distribution is crucial for ion transport, with larger pores (≥10–50 nm) facilitating ion movement, while smaller pores (<10 nm) reduce permeability and enhance durability [72]. The size of the pore "throat" and free water primarily influence transport rather than the hydrated chloride ion, which is about 0.3 nm (approximately 3Å). Closed pores (less than 20 nm) increase concrete density and decrease permeability [73,74]. In marine settings, chloride and sulfate ions produce secondary minerals like Friedel's salt and ettringite in concrete pores. These can decrease porosity and raise density, but also cause internal expansion and microcracks, reducing durability [75]. Their aluminosilicate gel matrix is more chemically stable, resulting in lower chloride diffusivity and better resistance to sulfate attack despite greater porosity [76]. Open pores allow more ions to enter, increasing corrosion risk, while closed pores block pathways and boost durability. Therefore, pore connectivity and chemistry matter more than total porosity. The superior performance of geopolymer concretes in marine conditions illustrates how a complex pore network and chemical stability can counteract the effects of increased pore volume. These findings highlight the need for concrete mixes with reduced porosity to limit ion diffusion and improve the durability of marine structures. Advanced mix designs and additives that reduce porosity significantly extend structural lifespan in marine environments. [19,40].

3.5 Analysis of Variance for Closed Porosity in Wrapping Mortars

This study analyzed the effects of RHA substitution and immersion time on closed porosity using ANOVA at a 95% confidence level. Tukey's post hoc test identified conditions that led to significant differences, highlighting the role of closed porosity in forming denser microstructures. The combined analysis provided insights into microstructural factors and helped identify optimal conditions for desired properties. **Table 6** shows the ANOVA results for RHA substitution and immersion time as independent factors.

Table 6. ANOVA analysis for closed porosity

Source	DF	Adj SS	Adj MS	F-Value	P-Value
RHA (%)	3	3.897	1.299	8.070	0.001
Immersion time (days)	5	59.102	11.820	73.400	0.000
RHA (%)*Immersion time (days)	15	12.554	0.837	5.200	0.000
Error	24	3.865	0.161		
Total	47	79.418			

Table 6 shows that RHA substitution, immersion time, and their interaction all have a statistically significant effect on closed porosity, with P-values of 0.001, 0.000, and 0.000, respectively. These low P-values indicate a strong statistical association between these factors and closed porosity outcomes.

The findings highlight that variations in RHA levels and immersion times, as well as their interaction, significantly influence the closed porosity of the materials. A factorial plot in **Fig. 17** visually illustrates the relationship between RHA substitution and immersion time on closed porosity. The factorial plot clearly illustrates how RHA substitution and immersion time interact to influence closed porosity. This graphical representation enhances the interpretation of statistical findings by illustrating the complex relationship between the two factors.

Fig. 17 also indicates that 5% RHA substitution results in the highest closed porosity, while 10% yields the lowest. Additionally, closed porosity increases with longer immersion times. In **Table 7** two groups were identified: Group A (0% and 5% RHA substitution), indicating statistically similar effects, and Group B (0%, 2.5%, and 10% RHA substitution), suggesting comparable impacts among these levels but differing from Group A.

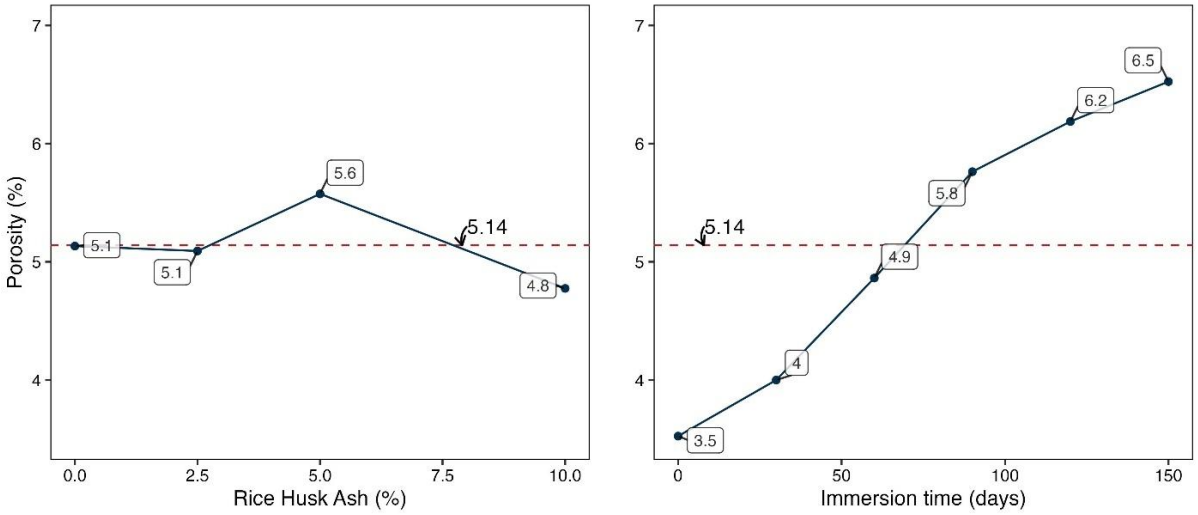

Fig. 17. The relation between RHA substitution and immersion time on closed porosity.

Table 7. Grouping information using the Tukey Method and 95% confidence (RHA effect on closed porosity)

RHA (%)	N	Mean	Grouping	
5.0	12	5.575	A	
0.0	12	5.133	A	B
2.5	12	5.092		B
10.0	12	4.775		B

Identification of four groups based on immersion time is presented in **Table 8**. Tukey's post hoc test results in **Table 7** and **Table 8** show distinct treatment groupings.

Table 8. Grouping information using the Tukey Method and 95% confidence (Immersion time effect)

Immersion time (days)	N	Mean	Grouping			
150	8	6.525	A			
120	8	6.188	A	B		
90	8	5.763		B		
60	8	4.863			C	
30	8	4.000				D
0	8	3.525				D

The 60-day treatment forms a distinct group with a significantly different response. Treatments at 120 and 150 days have similar effects, as do the 90- and 120-day groups and the 0- and 30-day groups. These results clarify how RHA levels and immersion durations influence closed porosity. The microstructure of geopolymer mortar varies with RHA content and immersion time, thereby altering pore properties and density. Fewer open pores result in a denser structure that restricts chloride

penetration. Therefore, ANOVA analysis identifies G5, containing 5% RHA, as the mixture with the optimal microstructural properties.

3.6 Chloride Penetration in Wrapping Mortars

Fig. 18 shows bound (left) and free (right) chloride penetration at the surface (M1) and 5 cm depth (M2) over 150 days of seawater immersion, accounting for the initial chloride in fly ash.

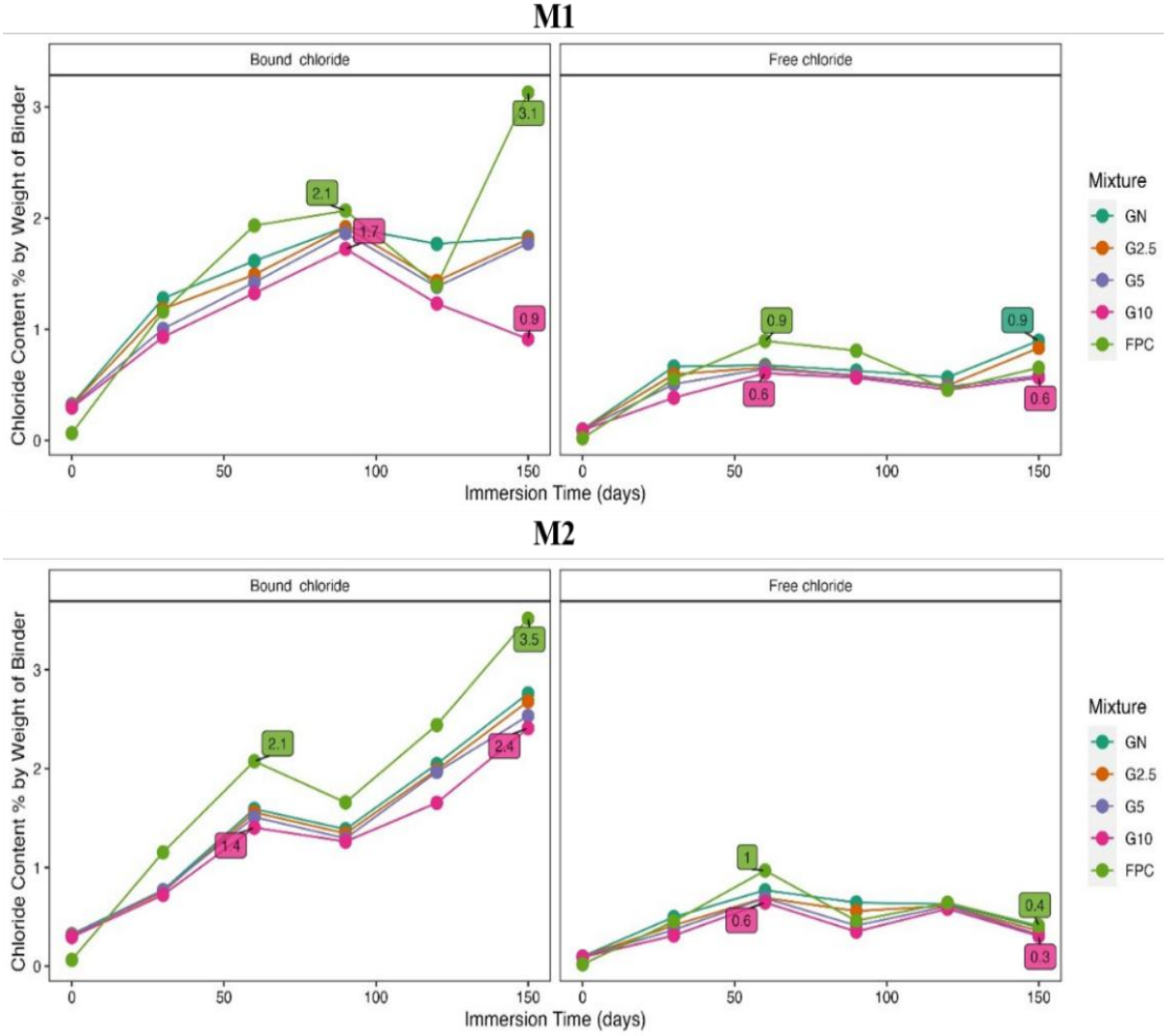

Fig. 18. The relation between RHA substitution and immersion time on closed porosity.

RHA addition reduced free chloride penetration, with concentrations decreasing over time as the pore structure densified during immersion. Increased density enhances impermeability, slowing chloride infiltration, while RHA's reactive silica further reduces open pores, limiting chloride entry. The chloride-binding capacity of geopolymer mortar is lower than that of FPC mortar, as seen at point M2. This is due to the absence of a chemical chloride-binding mechanism within the N-A-S-H gel system. In seawater, sodium ions can be released from the alumina-silica skeleton, especially at the mortar surface in contact with it, leading to depolymerization. Since sodium ions are loosely bound to alumina tetrahedra, their absence creates a negative charge that attracts positively charged ions such as sodium, magnesium, or potassium from seawater. This ion exchange primarily occurs at the mortar surface, allowing chloride ions to penetrate without altering the N-A-S-H structure. In less compact systems, alumina may also leach due to imbalances in [SiO_4] and [AlO_4] bonds. Chloride ions can bind to cations, such as Fe or Al, within geopolymer pores. However, in silica-rich systems, sodium leaching is reduced, and the Si-O-Si bonds remain intact, minimizing chloride ion entry. This is exemplified by G10, where chloride ions did not bind to the surface (M1) but penetrated the matrix (M2) due to the presence of

open pores. The protective geopolymer mortar formed C-A-S-H gel at the IC interface, reducing chloride penetration. **Fig. 19** shows a decline in chloride ion penetration into the IC for all geopolymer mortars over 30, 60, and 90 days.

G5 and G10 mortars with dense silica bonds had the lowest free chloride levels, whereas FPC mortar showed an increasing trend. In geopolymer systems, chloride ions bind physically to the gel surface, whereas in Portland concrete, they bind both physically and chemically to hydration products. N-A-S-H gel has a higher physical chloride-binding capacity than C-A-S-H gel [77,78]. It is reported that the combination of C-A-S-H and N-A-S-H forms a 3D structure that slows chloride diffusion [79]. Chloride binding in C-A-S-H gel occurs externally, resulting in lower chloride penetration, with its binding capacity surpassing that of C-S-H gel [80].

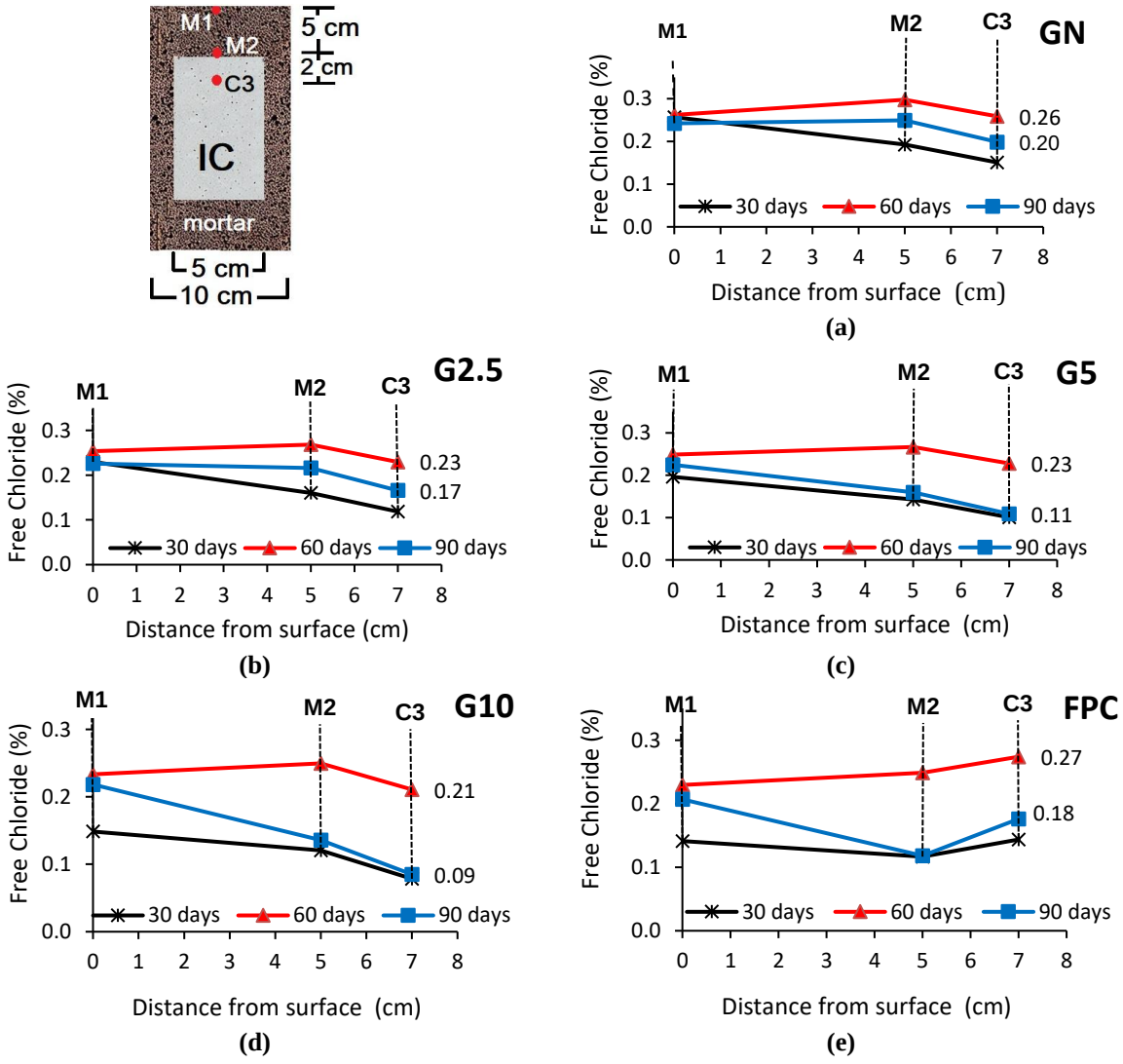

Fig. 19. Chloride content at different points from the surface during submersion.

3.7 Sulfate Attack

Fig. 20 shows sulfate penetration in G5 and FPC specimens at depths of 0, 5, and 7 cm after 30, 60, and 90 days of immersion. At point C3 (IC), sulfate content reached 0.72%, 1.27%, and 1.3% of the concrete weight, exceeding chloride content, which measured 0.31%, 0.72%, and 0.45% at the same times. A similar trend was observed in FPC mortar, with sulfate penetration at point C3 recorded at 2.15%, 1.25%, and 1.74%, compared to chloride levels of 0.51%, 0.86%, and 0.81%. **Fig. 5** shows that sulfate levels in Madura Strait seawater have risen from 2015 to 2025. The cumulative sulfate content during immersion reached 0.44%, classifying the exposure as severe (S2) per ACI 318-19, indicating a heightened risk of sulfate-induced deterioration of concrete durability compared to chloride attacks.

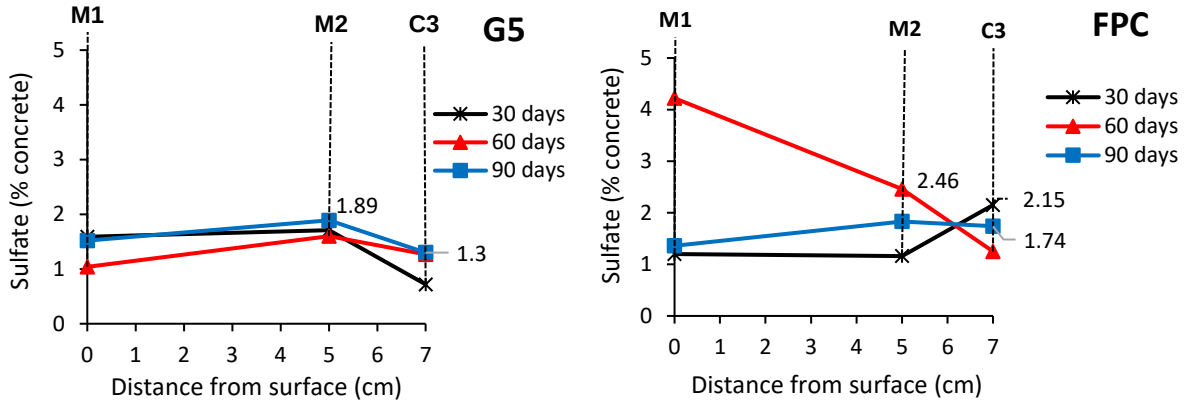

Fig. 20. Total sulfate in wrapping mortar and inside the IC at: G5 (left) and wrapping mortar FPC (right).

N-A-S-H surfaces can absorb both cations (Na, Mg, K, Ca) and anions from seawater. The cations pair with chloride and sulfate ions to form ionic pairs. However, the captured cations are larger than sulfate ions (SO_4^{2-}), causing the N-A-S-H layer to attract and accumulate chloride and sulfate ions.

This study shows that while 10M NaOH reduces chloride ingress, it may not fully block sulfate penetration into the IC. Higher alkalinity or finer FA and RHA particles could improve performance. Geopolymer mortar outperformed FPC in sulfate resistance, with the N-A-S-H and C-A-S-H gel cross-linking in the IC interlayer (M2) reducing sulfate penetration. FPC mortar relied on alumina-rich pozzolanic reactions to mitigate C-S-H decalcification. The findings suggest using FA and RHA with slag or metakaolin to enhance sulfate resistance, as Wang et al. [81] demonstrated improved impermeability with C-(N)-A-S-H gel formation.

It is reported that sulfate and magnesium attacks in a chloride environment degrade concrete, reducing Friedel's salt content [82]. Sulfate ions bind to the AFm phase, decreasing chloride binding capacity. The type and concentration of cations influence free chloride levels in concrete. Over time, in the geopolymer system, sulfate ions contribute to pore refinement and activate geopolymerization, leading to reduced chloride diffusion [83].

3.8 pH Change in Wrapping Mortar

Fig. 21 shows the pH values at points M1 and M2 in the mortar. The pH at M1, in direct contact with seawater, is slightly lower than at M2, indicating that cations react with negative ions in surface pores. Geopolymer mortar generally has a lower pH than Portland mortar, despite using a concentrated alkali solution. Increasing RHA content further lowers the pH, with GN at 12.3 and G10 at 11.9 before submersion. The geopolymerization process uses an alkaline solution to react with Al_2O_3 and SiO_2, reducing OH^- levels and lowering mortar pH during the first month of immersion. Prolonged immersion increases pH due to sodium ion leaching, which activates oxygen species in the N-A-S-H skeleton, attracting hydrogen atoms and forming hydroxyl groups at the ends of Si-Al bonds.

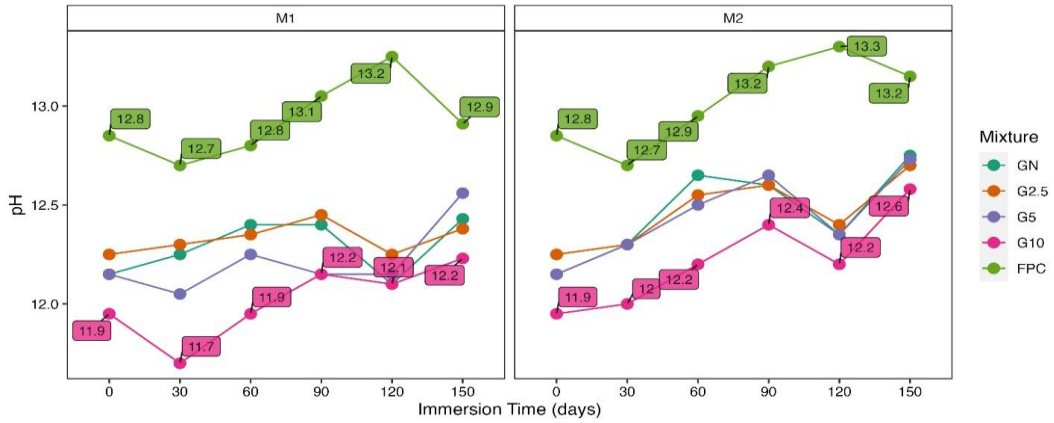

Fig. 21. pH at points M1 and M2 in wrapping mortar.

This pH fluctuation is influenced by the balance between hydroxyl formation and the strength of

Si-Al bonds. Chloride and sulfate ions in the geopolymer enhance the solubility and reactivity of FA, providing an advantage since the solubility of silica and alumina in FA is not solely dependent on hydroxide ions in the system. The breakdown of sodium ions increased the pH of the pore solution. However, the high sodium content in seawater reduced the risk of sodium leaching from the geopolymer mortar. To stabilize the pH, a highly alkaline solution, typically at least 10 M NaOH, is needed for geopolymer mixtures in contact with water.

At point M2, adjacent to the IC, the FPC mortar showed a pH increase from 12.9 (pre-soaking) to 13.3 after 120 days of immersion, followed by a slight decrease to 13.2 at 150 days. The observed increase in pH indicated a sulfate attack. The infiltration of sulfate ions decalcified the C-S-H gel, liberating Ca^{2+} and OH^- ions into the pore solution and subsequently elevating the pH. The decline in pH observed in the FPC mortar at 150 days was likely due to carbonation rather than sulfate or chloride exposure. This form of attack involved carbonate ions reacting with available free calcium to form calcite, or the deposition of dissolved calcite from seawater into the mortar's pores. Li et al. [84] found that the rate of pH decrease in concrete products was affected by the dilution level of CO_2 in seawater.

3.9 Carbonation

Increasing sulfate content in the Madura Strait indicates higher dissolved carbon in seawater, coinciding with increasing emissions in Surabaya, a large coastal city. Dissolved carbon ions in seawater can be adsorbed by concrete to form carbonate bonds. Carbonate ion measurements were taken at points M1, M2, and C3 after 150 days of immersion. The method used was acidimetric titration, which was also used by other studies [85,86] to measure the carbonate phase and quantify mineralized CO_2 in the wrapping mortars and the inner concrete. **Fig. 22** shows penetration of carbonate ions in G5 and FPC specimens at different depths after 90 days and 150 days of immersion. At 150 days of immersion, in mortar G5, mineralized carbonation reached 2.2% on the surface and 1.5% at M2. Higher carbonation in the geopolymer mortar shows that the geopolymer adsorbed more carbonate ions from seawater than the FPC mortar. The Na+ content of its matrix also influences the ability of geopolymer mortar to adsorb carbonate ions from seawater. As previously explained, during immersion, the pH of the geopolymer increases due to the solubility of Na ions, which likely bind to carbonate ions, precipitating in the mortar's pores. The result of this precipitation can be sodium carbonate (natrite) and/or calcium carbonate, since fly ash in this study contains free lime as well as the original Ca^{2+} ions from seawater. These minerals can be identified using XRD analysis.

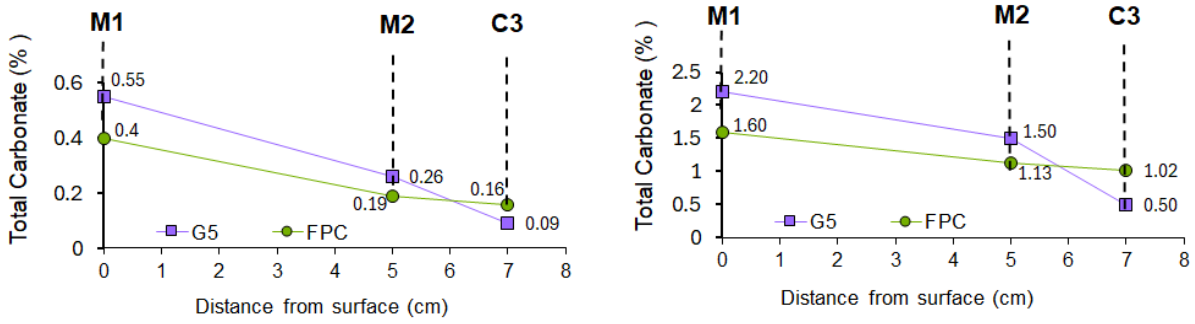

Fig. 22. Total mineralized carbonate (% binder weight) in wrapping mortar at 90d (left) and 150d (right).

All water that interacts with the atmosphere naturally absorbs carbon dioxide, playing a key role in the carbon cycle. As these waters traverse rocks and sediments, they pick up metal ions such as calcium and magnesium, yielding dilute bicarbonate solutions. Bicarbonate is the dominant form of dissolved inorganic carbon in both seawater and most freshwater, serving as a significant carbon sink that helps regulate environmental carbon levels. Biologically, attached biota, especially bacteria, barnacles, and microalgae, play an important role in accelerating carbonation through their metabolic activities. Autotrophic microorganisms such as cyanobacteria and microalgae carry out photosynthesis and assimilation of inorganic carbon (CO_2), producing carbonate ions (CO_3^{2-}) and bicarbonate (HCO_3^-) as by-products [87]. Heterotrophic bacteria like Bacillus, Pseudomonas, and Nitrosomonas increase dissolved CO_2 at the concrete–seawater interface through respiration and oxidation of organics. This CO_2 reacts with calcium ions in the concrete, resulting in the precipitation of calcium carbonate ($CaCO_3$) [88]. On the geopolymer surface, this mechanism is further enhanced by the presence of active Si–O–

Al and Na^+ sites, which adsorb dissolved CO_2 more efficiently than in Portland cement-based systems. Therefore, the increased carbonation in samples with biofouling reflects not only chemical degradation but also microbial biomineralization, which enriches the concrete surface layer with biological carbonate precipitation [89].

3.10 X-Ray Diffraction (XRD)

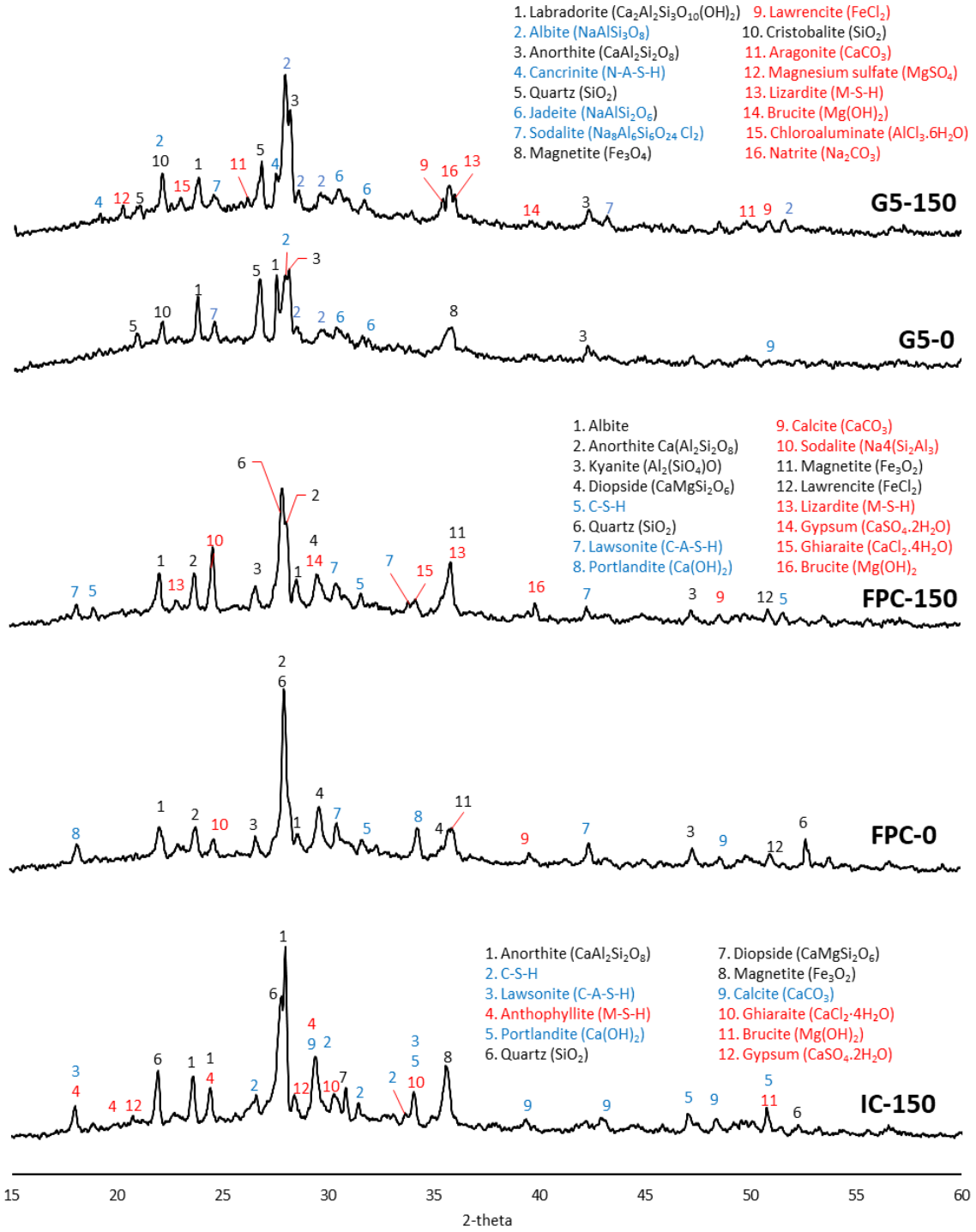

Fig. 23. XRD test result of specimens before and after immersion.

Fig. 23 shows the XRD patterns of G5 mortar (5% RHA), its IC, and FPC before and after 150 days of immersion. Before immersion in G5-0, geopolymerization forms minerals such as albite, jadeite, cancrinite, and sodalite. Cancrinite, a product of the FA and NaOH-based activator reaction represents the N-A-S-H gel phase. Lawrencite, containing chloride ions, originates from FA that contains Fe reacted with chloride ions, likely due to its seaside ash yard source. Labradorite, quartz, anorthite, and

magnetite come from fly ash and sand, while cristobalite derives from RHA. Native minerals are shown in black, geopolymerized or hydration minerals in blue, and minerals formed after seawater immersion in red. After seawater immersion, G5-150 showed reduced crystallinity of FA-derived minerals, such as labradorite and quartz, indicating continued geopolymerization. The high sodium content in seawater sustained the reaction and improved the solubility of FA and RHA. Additionally, there was a notable increase in geopolymerization minerals, especially albite and anorthite. Geopolymers absorb water due to hydroxyl groups, forming capillary pores. Increased albite content, from sodium ion leaching, relaxes Si-O-Al chains, triggering [AlO_4] and [SiO_4] repulsion and hydroxyl binding. Ion discharge into pore water promotes the formation of brucite ($Mg(OH)_2$), which increases pH. While brucite does not initiate geopolymerization, it stabilizes pH and improves mechanical properties. Intensified geopolymerization increased the Si/Al reaction rate, enhancing compressive strength from 45 MPa (G5-0) to 60 MPa (G5-150). The relaxation of [AlO_4] and [SiO_4] ions weakened bonds, forming Al products that bind to seawater anions, such as chloride, forming chloroaluminate. Simultaneously, Si binds with Mg or brucite, forming magnesium silicate hydrate (M-S-H). Chloride ions were captured in the system, forming compounds such as chloroaluminate with Al, sodalite with Si/Al, and lawrencite with iron.

Carbonate ions in the geopolymer system bind with sodium to form natrite and with calcium to form aragonite. The sodium involved comes from alkali-activator leaching and from unreacted sodium [90]. Dissolved alkalis from seawater diffuse through micropores, reacting with CO_2 to form carbonate precipitates. Seawater's calcium content promotes aragonite deposits, with higher calcium levels at the seabed than on the surface. Additionally, the formation of magnesium sulfate salts indicates seawater intrusion and precipitation within the geopolymer mortar.

The XRD results for G5 at point C3 in the IC show the formation of portlandite and C-S-H phases from cement hydration, while the pozzolanic reaction with 20% FA produced the C-A-S-H phase, represented by lawsonite. Minerals such as ghiaraite, anthophyllite (M-S-H), brucite, and gypsum were also detected, indicating that sulfate and chloride penetration reached the coated concrete, consistent with the chloride and sulfate penetration results in **Fig. 19** and **Fig. 20**. Magnesium sulfate penetration in core concrete led to portlandite decalcification, forming gypsum, and brucite reacted with silica from FA to form M-S-H. However, it did not negatively affect the IC concrete. Seo et al. [91] noted that gypsum formation increases with higher magnesium sulfate levels. Brucite and gypsum acted as pore fillers, sealing pores and limiting further ion penetration. This pore-filling effect from sulfate and chloride penetration contributed to the increased compressive strength of specimen G5.

The XRD results show the mineral composition of FPC mortar before (FPC-0) and after 150 days of seawater exposure (FPC-150). In FPC-0, cement hydration products include portlandite ($Ca(OH)_2$), C-S-H, and C-A-S-H, along with minerals from natural components such as anorthite, diopside, quartz, calcite, and magnetite. The FA used contained 0.32% bound chloride ions, forming sodalite and lawrencite ($FeCl_2$). After immersion, new minerals such as gypsum ($CaSO_4 \cdot 2H_2O$) and ghiaraite ($CaCl_2 \cdot 4H_2O$) formed due to the infiltration of chloride and sulfate ions, leading to the decalcification of portlandite and C-S-H. Calcium ions released into the pores bonded with sulfate ions, forming gypsum. While C-A-S-H gel resisted sulfate attack, chloride ions weakened its stability, leading to the formation of less durable Friedel's salt. Ghiaraite formation indicated early chloride attack, emphasizing the importance of limiting C_3A content and increasing SCMs to improve durability in aggressive environments.

Mg^{2+} ions in seawater, present as MgCl and $MgSO_4$ salts, react with $Ca(OH)_2$ in concrete to form brucite ($Mg(OH)_2$) and $CaSO_4$ or $CaCl_2$ [91,92]. Brucite formation leads to the decomposition of C-S-H into non-cohesive M-S-H [91] and, in excess, causes volume instability due to its expansive nature. Seawater immersion increased calcite formation, indicating carbonation, as calcium ions from hydration reacted with seawater carbonates, precipitating in pores [93]. Unlike aragonite in G5 mortar, calcite reflects the different calcium sources in FPC mortar. $Ca(OH)_2$ depletion also results from pozzolanic reactions that form C-S-H and C-A-S-H phases. FA substitution enhances these reactions, with alumina-silica in FA binding incoming chloride ions as sodalite and chloroaluminate.

An intriguing aspect is the carbonation observed in the mortar. The increased calcite levels after soaking indicate that carbonate ions bind to calcium sources in the mortar. Similarly, geopolymers exhibited carbonation via the precipitation of natrite and aragonite. Further research is needed to assess the combined effects of rising CO_2 emissions, carbonation, and chloride and sulfate penetration in

concrete. Evaluating CO_2 capture capacity is essential to determine its impact on concrete durability.

3.11 Scanning Electron Microscope (SEM) Analysis

Fig. 24 presents SEM analysis of initial GN mortar before submersion, showing dense N-A-S-H gels with sodalite containing chloride from FA.

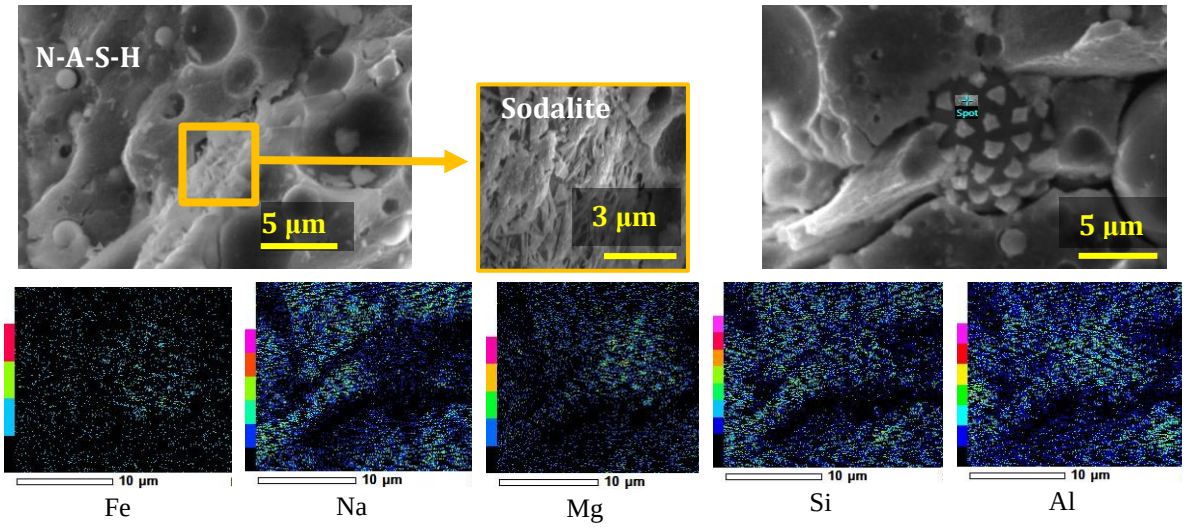

Fig. 24. SEM analysis of GN before submersion and its initial particles of Mg and Fe.

Another image of the same sample reveals unreacted fly ash particles at another spot, containing magnesium (Mg) and iron (Fe) micro-particles. These particles, primarily magnesium oxide and iron oxide (hematite or magnetite), originate from coal minerals and remain unbound due to the absence of sodium, indicating incomplete geopolymerization in that region. Elemental analysis at the spot shows Si (11.4%), Al (0.8%), Fe (9.1%), and Mg (6.1%), highlighting the dominance of Si and Fe and the notable presence of Mg.

The SEM test results at 2000× magnification in **Fig. 25** provide the results of GN mortar after immersion in seawater, depicting unreacted fly ash, reacted fly ash, magnesium sulfate, and lawrencite. The mineral lawrencite exhibits a layered structure in a trigonal system [30,65,94]. The deposition of magnesium sulfate on the N-A-S-H surface occurs as it precipitates from seawater into geopolymer pores. This pore-filling effect compacts the mortar, enhancing compressive strength by accelerating alumina dissolution within the N-A-S-H skeleton. The resulting compaction improves the mechanical properties of GN mortar.

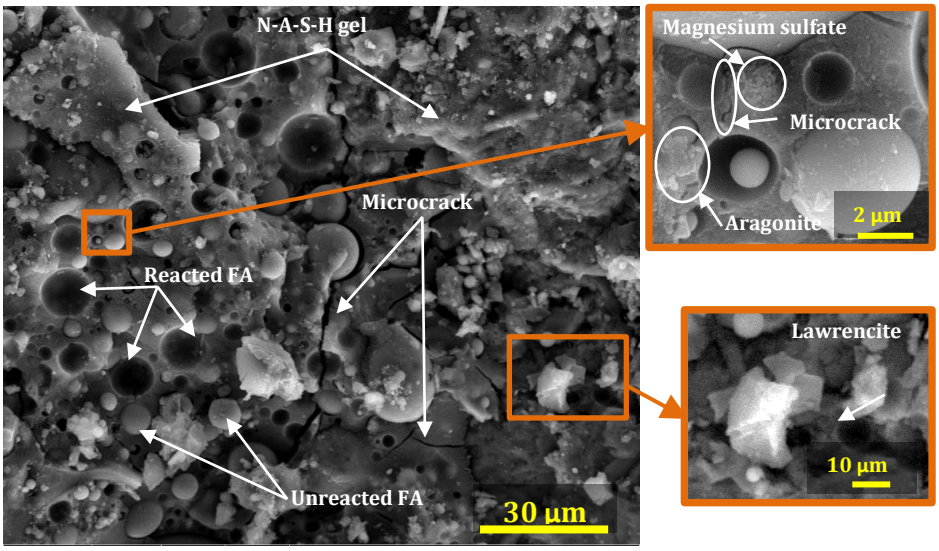

Fig. 25. SEM analysis for wrapping mortar GN after 150 days of submersion.

Fig. 26 shows SEM results of G5 mortar (2000× magnification) after 150 days of seawater immersion, identifying unreacted and reacted FA, cristobalite, and lawrencite.

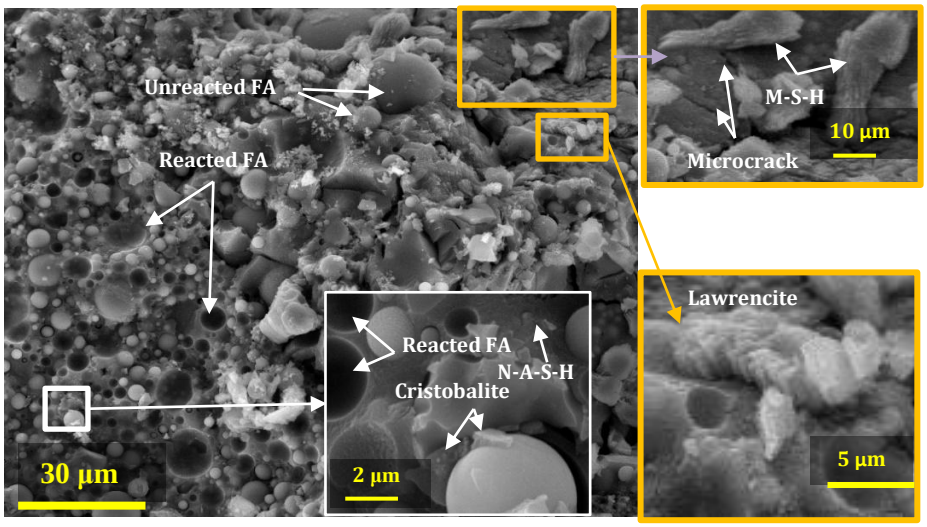

Fig. 26. SEM analysis for wrapping mortar G5 after 150 days of submersion.

Cristobalite from RHA enhances pore-filling, creating a denser matrix that reduces seawater penetration and limits magnesium sulfate deposits compared to GN mortar. In high Si/Al ratio systems (>2.25), magnesium sulfate can reactivate silica, forming an M-S-H gel that acts as a filler, reducing adhesion loss and expansive cracking. While cracks around N-A-S-H due to magnesium sulfate are present in both GN and G5 mortars, they are less severe in G2.5.

A higher sulfate addition rate posed a risk to the durability of concrete in seawater. While a 20% fly ash replacement improved durability, it was insufficient to prevent chloride and sulfate penetration from the FPC mortar into the IC. Additionally, a water-to-binder ratio above 40% and water content exceeding 200 kg/m³ proved ineffective. Using 10M NaOH in the wrapping mortar resulted in better durability than FPC mortar, reducing penetration of chloride and sulfate ions into the core concrete (IC), unlike the increasing trend observed in FPC mortar. However, 10M NaOH was less effective overall, suggesting that higher concentrations may be needed to accelerate FA and RHA dissolution and compact pores earlier.

3.12 Environmental Impact

The construction industry significantly contributes to resource consumption and CO_2 emissions. Incorporating secondary cementitious materials (SCMs), such as alkali-activated cements from industrial byproducts, can mitigate these impacts. While replacing cement with recycled concrete powder may initially reduce strength, proper treatment can achieve carbon-negative effects, promoting sustainability [95]. Reducing CO_2 emissions is crucial for achieving sustainability goals and combating climate change, especially in construction. This study demonstrates that geopolymer mortar emits significantly less carbon compared to Portland cement mortar. Although not entirely carbon-neutral due to alkali production emissions, geopolymer technology offers a sustainable alternative, reducing carbon emissions by approximately 30% in high-strength concrete compared to conventional cement [96].

Table 9. Materials emission factors ($kgCO_2$-eq/m^3) from references

Material	CO_2 emission factor	Minimum emission	Maximum emission
Fly Ash	0.009-0.027	Shi et al. [99]	Turner and Collins [100]
RHA	0.0027-0.1032	Fernando et al. [101]	Alnahhal et al. [102]
Cement	0.82-0.95	Collins [103]	Sun et al. [104]
Sand	0.014	Flower and Sanjayan [105]	Flower and Sanjayan [105]
Water	0.000318-0.00091	Zhao et al. [106]	Botto and Botto [107]
Na_2SiO_3	0.43-1.514	Zhang et al. [108]	Li et al. [109]
NaOH	0.625-1.425.	Thannimalay et al. [110]	Sandanayake et al. [97]

This study compares carbon emissions between geopolymer mortar and control mortar containing Portland cement (FPC). The CO_2 emission factors for the materials have been obtained from a range of scholarly references. Variability in these emission factors can be attributed to differences in production and transportation processes, as documented in some literature [97,98]. **Table 9,** 错误!书签自引用无

效。 and **Table 11** provide a comprehensive analysis of the reductions in carbon dioxide emissions associated with the use of geopolymer. The comparison is based on both the lowest and the highest CO_2 emission factors.

Table 10. Calculation of CO_2 emission ($kgCO_2$-eq/m^3) for wrapping mortars

Code	Calculation of CO_2 Emission-According to the lowest CO_2 emission factor							Total
	FA	RHA	Cement	Sand	Water	Na_2SiO_3	NaOH	
FPC	1.0	0.0	364.1	21.2	0.1	0.0	0.0	386.4
GN	7.6	0.0	0.0	13.8	0.0	104.1	21.3	146.8
G2.5	7.4	0.0	0.0	13.8	0.0	104.1	21.3	146.6
G5	7.2	0.1	0.0	13.8	0.0	104.1	21.3	146.5
G10	6.9	0.2	0.0	13.8	0.0	104.1	21.3	146.2

Table 11. Calculation of CO_2 emission ($kgCO_2$-eq/m^3) for wrapping mortars

Code	Calculation of CO_2 Emission-According to the highest CO_2 emission factor							Total
	FA	RHA	Cement	Sand	Water	Na_2SiO_3	NaOH	
FPC	3.0	0.0	421.8	21.4	0.2	0.0	0.0	446.4
GN	7.6	0.0	0.0	13.9	0.0	366.4	48.6	436.5
G2.5	7.4	1.9	0.0	13.9	0.0	366.4	48.6	438.2
G5	7.2	3.7	0.0	13.9	0.0	366.4	48.6	439.8
G10	6.9	7.4	0.0	13.9	0.0	366.4	48.6	443.2

The findings demonstrate that applying the lowest CO_2 emission factor (illustrated in **Fig. 27 (a)**) results in a 62% reduction in emissions from geopolymer mortar compared to control mortar. Additionally, incorporating Rice Husk Ash (RHA) further enhances this outcome, resulting in a 62.2% reduction in total emissions. This improvement is primarily due to RHA's ability to replace a portion of the fly ash, which exhibits a higher emission factor. In contrast, with calculations based on the highest emission factor, the significant reduction in emissions is no longer apparent (illustrated in **Fig. 27 (b)**). Carbon emission reductions are observed at only 2.2%, and emissions increase when RHA is utilized, due to its higher emission factor. The factor that significantly influences the increase in carbon emissions in geopolymers is sodium silicate. This is because sodium silicate production involves melting silica sand and soda ash at temperatures around 1400 °C, which consumes very high energy [100]. In general, geopolymer mortar can still reduce CO_2 emissions compared to traditional Portland cement (FPC) mortar [111]. However, producing rice husk ash (RHA) through burning may slightly increase emissions. While geopolymer synthesis emits less CO_2 than conventional cement, the production of alkali reagents still contributes to emissions, underscoring the need for further innovation in sustainable materials. Additionally, the use of industrial byproducts presents challenges, including regulatory acceptance and the need for continued research to optimize performance in construction applications.

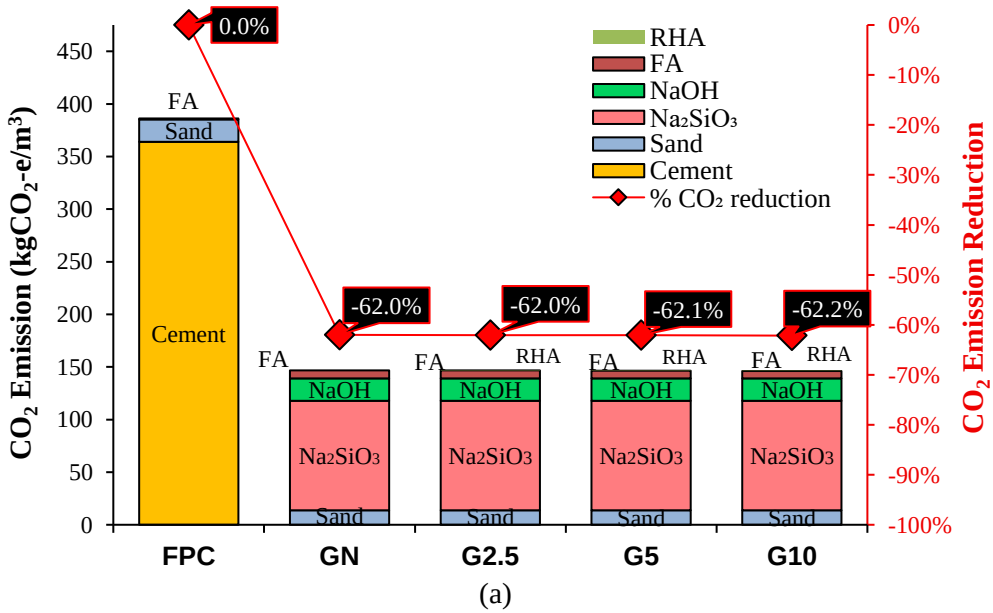

(a)

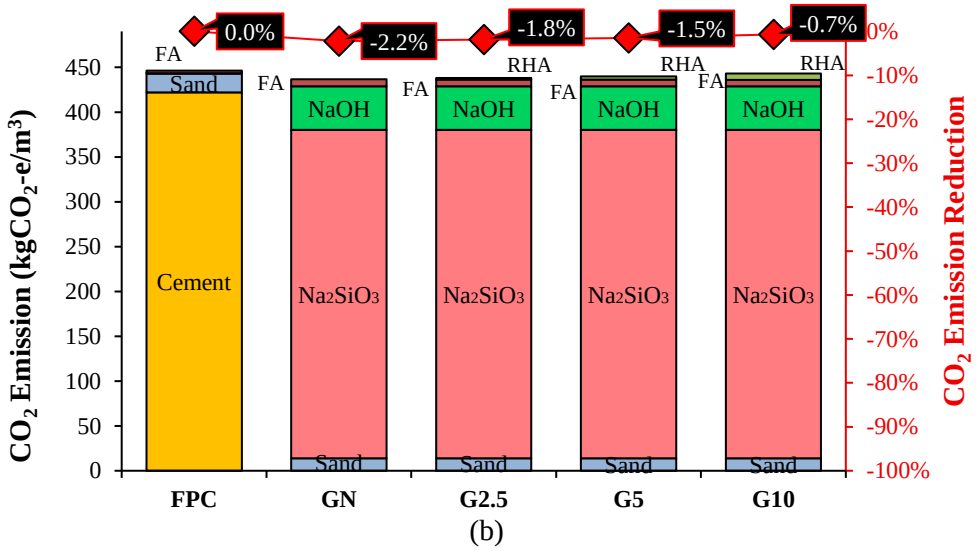

Fig. 27. CO_2 reduction of each geopolymer mortar variation compared to FPC mortar (a) Calculation based on the smallest emission factor (b) Calculation based on the highest emission factor.

Numerous studies on fly ash-based geopolymer systems have demonstrated potential reductions in CO_2 emissions of 36% to 64% compared to ordinary Portland cement (OPC). These reductions are influenced by various factors, including the type of activator, the curing temperature, and the distance the materials are transported. The findings from this study align well with the existing literature, highlighting the promising opportunity to enhance the environmental performance of geopolymer-based materials by partially substituting fly ash with rice husk ash (RHA). This innovative approach not only uses two local waste materials fly ash and RHA but also paves the way for a more sustainable, environmentally friendly construction industry by effectively reducing the carbon footprint of building materials.

4 Future Studies and Applications of Geopolymer Mortar in Marine Environments

The results of the study suggest that geopolymer mortar could be effectively used for a variety of applications, including jacketing, repairing, or patching existing concrete structures in challenging marine settings. This innovative method not only addresses the immediate needs of maintenance and restoration but also accounts for the ever-changing environmental conditions characteristic of such dynamic environments. These conditions are influenced by a multitude of factors, including tidal movements and atmospheric exposure, which can accelerate deterioration from salt spray and humidity. Furthermore, the presence of biofouling organisms that attach to submerged surfaces adds another layer of complexity to the maintenance of marine structures, as these organisms can degrade materials over time. By using geopolymer mortar, known for its durability and resistance to harsh marine environments, engineers and construction professionals can enhance the longevity and structural integrity of concrete elements exposed to these conditions. This approach not only promotes sustainability by utilizing eco-friendly materials but also represents a proactive strategy in the ongoing effort to preserve vital infrastructure in coastal and marine environments.

Further research on the application of geopolymer mortar in marine infrastructure should thoroughly assess its long-term durability, explore its self-healing properties, and evaluate the integration of alternative precursors and advanced nanomaterials to enhance resistance to sulfate and chloride exposure.

Further investigation into the self-healing capabilities of geopolymer mortar is required, as this material is intended to serve as a protective barrier for existing structures. Wave impact, seawater splash, and impurities in seawater can complicate the healing of cracks in geopolymer. Some types of seawater bacteria accelerate corrosion, requiring early crack healing before microbial initiation of corrosion [112]. However, the natural formation of calcium carbonate and brucite within the geopolymer matrix enables self-healing. In addition, carbonization and rehydration are the main self-healing mechanisms for microcracks (less than 300 μm). An interesting study showed that brucite has the potential to serve as the primary self-healing product precipitated in the gap to fill cracks [113]. The observations indicated

that seawater impurities are attached to the crack surface, potentially hindering crack self-healing. Adding lime, such as dolomite, to the geopolymer mortar mixture may be an interesting option for further study. Furthermore, the use of urease-producing bacteria, which are resistant to seawater and have a carbonic anhydrase effect, could aid the healing process [114]. These microbes produce precipitation material much more rapidly than natural precipitation does, driven by chemical reactions within the geopolymer mortar. Developing self-healing geopolymer composites employing bacteria or encapsulated healing agents warrants examination to improve crack resistance and prolong service life.

Exploring hybrid geopolymer coatings that integrate nano silica, graphene oxide, basalt fibers, or bio-based additives may further enhance geopolymer mortar's mechanical strength, impermeability, and adhesion in extreme marine environments [115]. The low surface roughness achieved with nanomaterials contributes to increased anti-fouling efficacy [42]. It also results in a more hydrophobic surface. The results clearly confirm that this combination allows for increased resistance to biofouling and biodeterioration of durable concrete structures in aggressive marine environments [116].

The practical implementation of geopolymer coatings on coastal and offshore structures requires pilot-scale trials under diverse tidal conditions to assess performance over prolonged exposure to seawater, temperature variations, and wet-dry cycles. In the context of Indonesia's New Capital City (IKN), where infrastructure development is projected to occur near coastal regions characterized by aggressive sulfate-rich conditions, geopolymer mortar emerges as a sustainable alternative to conventional coatings, thereby reducing carbon emissions and enhancing structural durability [117]. Furthermore, applying geopolymer mortar in seawalls, piers, marine tunnels, and offshore wind turbine foundations could bolster Indonesia's initiatives for climate adaptation and green infrastructure development. Conducting life cycle assessments (LCAs) alongside techno-economic feasibility studies is crucial for improving cost-effectiveness and enabling mass production. This will ascertain that geopolymer technology is a viable and sustainable option for next-generation marine infrastructure. The proposed future studies and applications are illustrated in **Fig. 28**.

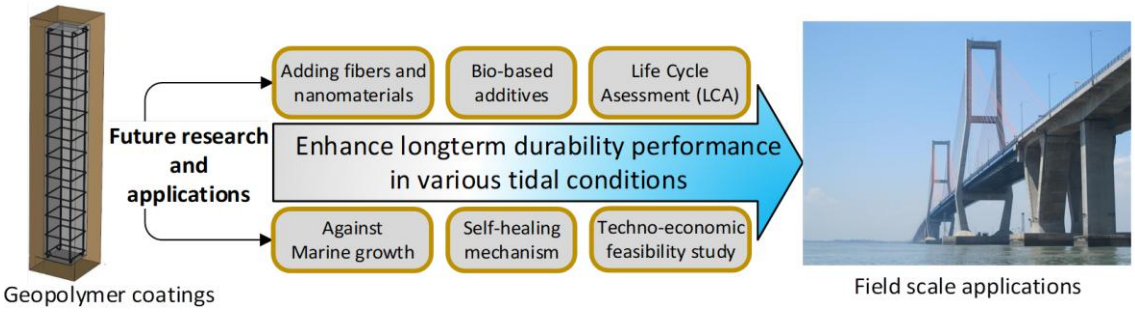

Fig. 28. Future studies should focus on enhancing the durability of structures in coastal areas.

5 Conclusions

This study provides insights into the performance of geopolymer mortar despite some limitations. These limitations highlight the need for future investigation. The 5-month immersion period may not reflect long-term durability, and findings are specific to the materials and seawater used. Comparisons are limited to FPC mortar and exclude other coatings. Further research is needed, including a lifecycle assessment and real-world application testing. The findings also indicated that geopolymer mortar has potential for use in jacketing, repairing, or patching existing concrete structures in marine environments. This approach reflects the dynamic nature of environmental conditions, which fluctuate due to factors such as tidal action, wave splash, atmospheric exposure, and biofouling. While a 5% RHA replacement is optimal, achieving 62.1% of the total emission reduction, investigating other silica-rich materials could further improve performance. Key findings of this study emphasize the feasibility of utilizing waste materials for protecting existing Portland concrete structures and include the following conclusions:

1) The geopolymer mortar formed a strong bond with the Portland product surface, facilitated by the infiltration of geopolymer gel and unreacted fly ash into IC pores, reacting with available calcium. Despite the IC's 28-day age, the geopolymer coating formed calcium aluminosilicate hydrate (C-A-S-H) minerals at the interface, thereby creating a chemical bond. This bond enhanced mechanical properties and established a robust protective barrier against sulfate

attacks, significantly contributing to the geopolymer's durability and resilience in aggressive environments.

2) The geopolymerization reaction occurring during the soaking period led to an increase in the density of the geopolymer mortar, resulting in enhanced compressive strength of the specimens. G10 showed the largest increase, rising by 78%. The 28-day compressive strengths of GN, G2.5, G5, and G10 were 40 MPa, 42 MPa, 45 MPa, and 27 MPa, respectively. After 150 days of soaking, these strengths increased to 62 MPa, 58 MPa, 60 MPa, and 48 MPa, respectively. In contrast, the compressive strength of the inner concrete (IC) wrapped in FPC mortar initially peaked at 60 days of immersion and then declined.

3) Although burning rice husks slightly elevates the CO_2 content in RHA material, it has been demonstrated to serve as a silica source for enhanced geopolymerization reactions during seawater immersion, leading to increased closed pores, reduced total porosity and chloride ingress, and improved compressive strength. ANOVA results also supported this. Higher silica availability increased the Si/Al ratio, compacting the Si-O-Al skeleton and enhancing stability during 150 days of seawater immersion. Using up to 10% RHA to replace the volume of FA resulted in decreased compaction, increased mortar porosity, and reduced compressive strength. Therefore, the recommended RHA level is 5% of the FA volume, as implemented in mortar G5.

4) RHA significantly reduced chloride ion penetration in geopolymer mortar, with G10 showing the lowest penetration. However, free chloride ions still permeated due to high open porosity. The chloride-binding capacity of geopolymer mortar was lower than that of FPC, as the N-A-S-H surface exhibited a less effective binding mechanism. Chloride ions primarily bonded with Fe to form lawrencite and with Al to form chloroaluminate, both trapped in the micropores of the geopolymer gel.

5) Sulfate attack on the protective mortar was noted, with geopolymer mortar showing better sulfate retention. Sulfate binding involved cations such as magnesium, as Mg^{2+} reacted with hydroxyl groups on the Si-O-Al chain to form brucite, which then reacted with silica to produce M-S-H. Dissolved silica from RHA helped mitigate magnesium damage. However, sulfate settled in pores as magnesium sulfate, causing internal microcracks. Overall, sulfate ion attacks were more damaging to geopolymer mortar than chloride ions.

6) Chloride and sulfate attacks did not affect the geopolymerization process (N-A-S-H gel) but led to the degradation of cement hydration products such as C-S-H, C-A-S-H, and $Ca(OH)_2$. Geopolymer mortar consistently exhibited a lower pH than FPC mortar. Minor pH fluctuations during immersion reflected changes in mineral composition due to ion attack. In geopolymers, sodium ion leaching activates oxygen species within the N-A-S-H framework, forming hydroxyl groups (brucite). In contrast, FPC showed an increase in pH due to sulfate-induced decalcification of the C-S-H gel, which released Ca^{2+} and OH^- ions into the pore solution.

CRediT authorship contribution statement

Januarti Jaya Ekaputri: Conceptualization, Methodology, Software, Supervision, Visualization, Validation, Writing – original draft, Writing – review & editing. **Chlarisya Eka Ningtyas:** Formal analysis, Investigation, Writing – review & editing, Software. **Iqlima Nuril Amini:** Project administration, Writing- review & editing. **Pitcha Jongvivatsakul:** Investigation, Writing – review & editing. **Tidarut Jirawattanasomkul:** Resources, Validation. **Himawan Tri Bayu Murti Petrus:** Conceptualization, Data curation, Visualization. **Rita Irmawaty:** Investigation, Validation. **Fakhruddin:** Data curation, Visualization. **Ari Widayanti:** Project administration, Resources**. Retno Trimurtiningrum:** Formal analysis, Validation. **Yuya Takahashi:** Methodology, Validation, Writing – review & editing

Declaration of competing interests

The authors declare that they have no known competing financial interests or personal relationships that could have influenced the work reported in this paper.

Acknowledgement

The authors gratefully acknowledge financial support for our preliminary research from the Ministry of Higher Education, Science, and Technology of the Republic of Indonesia under the BIMA program for Applied Research - Output Prototype (Contract No. 2045/PKS/ITS/2026). The authors also extend their gratitude to Tanjung Jati B Power Plant for the valuable assistance in supplying fly ash for this study. A portion of the preliminary investigations conducted by Dr. Ekaputri was supported by the HETI-ADB Project Loan Nomor 4110-INO, Institut Teknologi Sepuluh Nopember, 2024, through RKI No. 0007/01.PK/PPK-HETI/ITS/2024 and the ITS Center Collaboration Research No. 20251950/PKS/ITS/2025

References

[1] Noushini A, Castel A, Aldred J, Rawal A. Chloride diffusion resistance and chloride binding capacity of fly ash-based geopolymer concrete. Cement and Concrete Composites 2020; 105:103290: 1–19. https://doi.org/10.1016/j.cemconcomp.2019.04.006

[2] Wang Y, Ueda T, Gong F, Zhang D. Meso-scale mechanical deterioration of mortar due to sodium chloride attack. Cement and Concrete Composites 2019; 96: 163–173. https://doi.org/10.1016/j.cem concomp 2018. 11.021

[3] Ding Q, Yang J, Hou D, Zhang G. Insight on the mechanism of sulfate attacking on the cement paste with granulated blast furnace slag: an experimental and molecular dynamics study. Construction and Building Materials 2018; 169: 601–611. https://doi.org/10.1016/j.conbuildmat.2018.02.148

[4] Gupta S, Chaudhary S. State of the art review on supplementary cementitious materials in India – II: characteristics of SCMs, effect on concrete and environmental impact. Journal of Cleaner Production 2022; 357. https://doi.org/10.1016/j.jclepro.2022.131945

[5] Nayak DK, Abhilash PP, Singh R, Kumar R, Kumar V. Fly ash for sustainable construction: a review of fly ash concrete and its beneficial use case studies. Cleaner Materials 2022; 6. https://doi.org/10.1016/j.clema.2 022.100143

[6] Fernando S, Gunasekara C, Law DW, Nasvi MCM, Setunge S, Dissanayake R. Assessment of long term durability properties of blended fly ash–rice husk ash alkali activated concrete. Construction and Building Materials 2023; 369. https://doi.org/10.1016/j.conbuildmat.2023.130449

[7] Chalee W, Cheewaket T, Jaturapitakkul C. Enhanced durability of concrete with palm oil fuel ash in a marine environment. Journal of Materials Research and Technology 2021; 13: 128–137. https://doi.org/10.1016/j.jm rt.2021.04.061

[8] Sahoo S, Parhi PK, Chandra Panda B. Durability properties of concrete with silica fume and rice husk ash. Cleaner Engineering and Technology 2021; 2. https://doi.org/10.1016/j.clet.2021.100067

[9] Chalee W, Teekavanit M, Kiattikomol K, Siripanichgorn A, Jaturapitakkul C. Effect of w/c ratio on covering depth of fly ash concrete in marine environment. Construction and Building Materials 2007; 21(5): 965–971. https://doi.org/10.1016/j.conbuildmat.2006.03.002

[10] Pasupathy K, Singh Cheema D, Sanjayan J. Durability performance of fly ash-based geopolymer concrete buried in saline environment for 10 years. Construction and Building Materials 2021; 281. https://doi.org/10 .1016/j.conbuildmat.2021.122596

[11] Sadati S, Arezoumandi M, Shekarchi M. Long-term performance of concrete surface coatings in soil exposure of marine environments. Construction and Building Materials 2015; 94: 656–663. https://doi.org/1 0.1016/j.conbuildmat.2015.07.094

[12] Alyousef R, Ebid AAK, Huseien GF, Mohammadhosseini H, Alabduljabbar H, Ngian SP, Mohamed AM. Effects of sulfate and sulfuric acid on efficiency of geopolymers as concrete repair materials. Gels 2022; 8(1). https://doi.org/10.3390/gels8010053

[13] Petcherdchoo A. Pseudo-coating model for predicting chloride diffusion into surface-coated concrete in tidal zone: time-dependent approach. Cement and Concrete Composites 2016; 74: 88–99. https://doi.org/10.1016 /j.cemconcomp.2016.08.009

[14] Khanzadeh Moradllo M, Shekarchi M, Hoseini M. Time-dependent performance of concrete surface coatings in tidal zone of marine environment. Construction and Building Materials 2012; 30: 198–205. https://doi.or g/10.1016/j.conbuildmat.2011.11.044

[15] Amran M, Debbarma S, Ozbakkaloglu T. Fly ash-based eco-friendly geopolymer concrete: a critical review of the long-term durability properties. Construction and Building Materials 2020; 270. https://doi.org/10.10 16/j.conbuildmat.2020.121857

[16] Ekaputri JJ, Mutiara IS, Nurminarsih S, Chanh NV, Maekawa K, Setiamarga DHE. The effect of steam curing on chloride penetration in geopolymer concrete. MATEC Web of Conferences 2017; 138. https://doi.org/10.
1051/matecconf/201713801019

[17] Fu C, Ye H, Zhu K, Fang D, Zhou J. Alkali cation effects on chloride binding of alkali-activated fly ash and metakaolin geopolymers. Cement and Concrete Composites 2020; 114: 103721. https://doi.org/10.1016/j.ce

mconcomp.2020.103721
[18] Zerfu K, Ekaputri JJ. Nonlinear finite element study on element size effects in alkali-activated fly ash based reinforced geopolymer concrete beam. Case Studies in Construction Materials 2021; 15. https://doi. org/10. 1016/j.cscm.2021.e00765
[19] Zhang Z, Yao X, Zhu H. Potential application of geopolymers as protection coatings for marine concrete II. Microstructure and anticorrosion mechanism. Applied Clay Science 2010; 49(1–2): 7–12. https://doi.org/10. 1016/j.clay.2010.04.024
[20] Lyu X, Robinson N, Elchalakani M, Johns ML, Dong M, Nie S. Sea sand seawater geopolymer concrete. Journal of Building Engineering 2022; 50. https://doi.org/10.1016/j.jobe.2022.104141
[21] Thenmozhi R, Vijaya Prabha C. A study of alkali-activated coatings durability assessment in different environments. Polish Journal of Environmental Studies 2023; 32(4): 3323–3337. https://doi.org/10.15244/pj oes/162547
[22] Biondi L, Perry M, Vlachakis C, Wu Z, Hamilton A, McAlorum J. Ambient cured fly ash geopolymer coatings for concrete. Materials 2019; 12(6). https://doi.org/10.3390/ma12060923
[23] Trimurtiningrum R, Ekaputri JJ. Geopolymer grout material. Materials Science Forum 2016; 841: 40–47. ht tps://doi.org/10.4028/www.scientific.net/MSF.841.40
[24] Abdullah MMAB, Tahir MFM, Tajudin MAFMA, Ekaputri JJ, Bayuaji R, Khatim NAM. Study on the geopolymer concrete properties reinforced with hooked steel fiber. IOP Conference Series: Materials Science and Engineering 2017; 267. https://doi.org/10.1088/1757-899X/267/1/012014
[25] Zerfu K, Ekaputri JJ. Bond strength in PVA fibre reinforced fly ash-based geopolymer concrete. Magazine of Civil Engineering 2021; 101(1). https://doi.org/10.34910/MCE.101.5
[26] Nastiti SF, Ekaputri JJ. Effect of chloride ions on concrete with geopolymer coatings in coastal area. IOP Conference Series: Earth and Environmental Science 2020; 506. https://doi.org/10.1088/1755-1315/506/1/0 12043
[27] Chen S, Ruan S, Zeng Q, Liu Y, Zhang M, Tian Y, Yan D. Pore structure of geopolymer materials and its correlations to engineering properties: a review. Construction and Building Materials 2022; 328: 127064. htt ps://doi.org/10.1016/j.conbuildmat.2022.127064
[28] Kordi M, Farrokhi N, Pech-Canul MI, Ahmadikhah A. Rice husk at a glance: from agro-industrial to modern applications. Rice Science 2023. https://doi.org/10.1016/j.rsci.2023.08.005
[29] Hashim N, Ali MM, Mahadi MR, Abdullah AF, Wayayok A, Kassim MSM, Jamaluddin A. Smart farming for sustainable rice production: an insight into applications, challenges and future prospects. Rice Science 2023. https://doi.org/10.1016/j.rsci.2023.08.004
[30] FAOSTAT. Production/yield quantities of rice in world (1994–2020). https://www.fao.org/faostat/en/#data/QC/visualize, 2023 (accessed 20 November 2025).
[31] Badan Pusat Statistik. Berita resmi statistik No. 74/10/Th.XXV. https://www.bps.go.id/id/pressrelease/2022/ 10/17/1910/pada-2022--luas-panen-padi-diperkirakan-sebesar-10-61-juta-hektare-dengan-produksi-sekitar- 55-67-juta-ton-gkg.html, 2022 (accessed 20 November 2025).
[32] Jindal BB, Jangra P, Garg A. Effects of ultra fine slag as mineral admixture on the compressive strength, water absorption and permeability of rice husk ash based geopolymer concrete. Materials Today: Proceedings 2020; 32: 871–877. https://doi.org/10.1016/j.matpr.2020.04.219
[33] Zhu H, Zhai M, Liang G, Li H, Wu Q, Zhang C, Hua S. Experimental study on the freezing resistance and microstructure of alkali-activated slag in the presence of rice husk ash. Journal of Building Engineering 2021; 38. https://doi.org/10.1016/j.jobe.2021.102173
[34] Ekaputri JJ, Ruitan XDE A, Petrus HTBM, Anda M, Purbawinasta LH, Laory I, Setiamarga DHE, Chijiwa N, Fujiyama C. Utilization of high-volume fly ash in pervious concrete mixtures for mangrove conservation. Resources Conservation and Recycling Advances 2024; 21. https://doi.org/10.1016/j.rcradv.2024.200204
[35] Specification for coal fly ash and raw or calcined natural pozzolan for use in concrete. https://doi.org/10.15 20/C0618-19
[36] Pradhan P, Dwibedy S, Pradhan M, Panda S, Panigrahi SK. Durability characteristics of geopolymer concrete-progress and perspectives. Journal of Building Engineering 2022; 59. https://doi.org/10. 1016/j.job e.2022.105100
[37] ASTM International. Standard test method for flow of hydraulic cement mortar. Book of Standards 2020; 04.01: C1437-20. https://doi.org/10.1520/C1437-20
[38] ACI Committee 357. Guide for design and construction of waterfront and coastal concrete marine structures-Guide (ACI PRC-357.3-14). American Concrete Institute, USA, 2014
[39] Nastiti SF, Ekaputri JJ, Sulton M, Rahardjo B, Rahma DY, Handayani AF, Wulandari FF. Corrosion rate and weight loss of geopolymer mortar coated concrete specimens with different thicknesses. 2023; 445. https://d
oi.org/10.1051/e3sconf/202344501025
[40] Annamalaisamy Sannasiraj RD, Shi S, Liu X, Gryllias K, Vandepitte D, Chronopoulos D, Zhang L. A fully coupled depth-dependent corrosion model for reinforced concrete piles under marine environmental

conditions. Construction and Building Materials 2025; 472. https://doi.org/10.1016/j.conbuildmat.2025.140795

[41] Li S, Jin Z, Pang B, Li J. Durability performance of an RC beam under real marine all corrosion zones exposure for 7 years. Case Studies in Construction Materials 2022; 17. https://doi.org/10.1016/j.cscm.2022.e01516

[42] Perdanawati RA, Risdanareni P, Setiamarga DHE, Ekaputri JJ. The effect of biofouling on cement based concrete substrate: insights from microfouling and macrofouling growth. 2025; 157. https://doi.org/10.1051/bioconf/202515706001

[43] ACI Committee 319. Building code requirements for structural concrete and commentary (ACI 318-19). American Concrete Institute, USA, 2019

[44] Halim LN, Ekaputri JJ, Triwulan. The influence of salt water on chloride penetration in geopolymer concrete. MATEC Web of Conferences 2017; 97. https://doi.org/10.1051/matecconf/20179701002

[45] Bediako M, Kevern JT, Amankwah EO. Effect of curing environment on the strength properties of cement and cement extenders. Materials Sciences and Applications 2015; 6(1): 33–39. https://doi.org/10.4236/msa.2015.61005

[46] Ozer B, Ozkul MH. The influence of initial water curing on the strength development of ordinary Portland and pozzolanic cement concretes. Cement and Concrete Research 2004; 34(1): 13–18. https://doi.org/10.1016/S0008-8846(03)00185-6

[47] Chen Y, Zhang Z, Liu Z, Ye P. Experimental analysis on mechanical properties of sea sand geopolymer recycled aggregate concrete. Construction and Building Materials 2024; 457. https://doi.org/10.1016/j.conbuildmat.2024.139421

[48] Perdanawati RA, Risdanareni P, Setiamarga DHE, Ekaputri JJ, Kusbiantoro A, Liao M-C. The potential of seawater in geopolymer mixtures: effect of alkaline activator, seawater, and steam curing on the strength of geopolymer paste.

[49] ASTM International. Standard test method for density, absorption, and voids in hardened concrete. Book of Standards 2013; 04.02 : C642-13. https://doi.org/10.1520/C0642-13

[50] Mehta A, Siddique R. Sustainable geopolymer concrete using ground granulated blast furnace slag and rice husk ash: strength and permeability properties. Journal of Cleaner Production 2018; 205: 49–57. https://doi.org/10.1016/j.jclepro.2018.08.313

[51] Wijaya AL, Ekaputri JJ, Triwulan. Factors influencing strength and setting time of fly ash based-geopolymer paste. MATEC Web of Conferences 2017; 138. https://doi.org/10.1051/matecconf/201713801010

[52] Kang SH, Hong SG, Moon J. The use of rice husk ash as reactive filler in ultra-high performance concrete. Cement and Concrete Research 2019; 115: 389–400. https://doi.org/10.1016/j.cemconres.2018.09.004

[53] Ouattara S, Sawadogo Y, Sawadogo M, Sorgho B, Seynou M, Blanchart P, Zerbo L. Effect of rice husk ash on physical, mechanical, and hydric properties of clay-based geopolymer. Results in Materials 2025; 28: 100821. https://doi.org/10.1016/j.rinma.2025.100821

[54] Gunasekara C, Law DW, Setunge S. Long term permeation properties of different fly ash geopolymer concretes. Construction and Building Materials 2016; 124: 352–362. https://doi.org/10.1016/j.conbuildmat.2016.07.121

[55] Ekaputri JJ, Triwulan, Junaedi S, Fansuri, Aji RB. Light weight geopolymer paste made with Sidoarjo mud (Lusi). 2015; 803: 63–74. https://doi.org/10.4028/www.scientific.net/MSF.803.63

[56] Verma P, Goldar D, Daniyal M, Singh SK. Effect of rice husk ash on the properties and performance of geopolymer concrete. SSRG International Journal of Civil Engineering 2024; 11(11): 11–22. https://doi.org/10.14445/23488352/IJCE-V11I11P102

[57] Wang T, Ishida T, Gu R, Luan Y. Experimental investigation of pozzolanic reaction and curing temperature-dependence of low-calcium fly ash in cement system and Ca-Si-Al element distribution of fly ash-blended cement paste. Construction and Building Materials 2021; 267. https://doi.org/10.1016/j.conbuildmat.2020.121012

[58] Li X, Xu F, Chen B, Li B, Chen Z, Zhu J, Peng C, Lin J. Investigation on the chloride ion erosion mechanism of cement mortar in coastal areas: from experiments to molecular dynamics simulation. Construction and Building Materials 2022; 350: 128810. https://doi.org/10.1016/j.conbuildmat.2022.128810

[59] Maes M, De Belie N. Resistance of concrete and mortar against combined attack of chloride and sodium sulphate. Cement and Concrete Composites 2014; 53: 59–72. https://doi.org/10.1016/j.cemconcomp.2014.06.013

[60] Purwanto, Ekaputri JJ, Nuroji, Indriyantho BR, Han A, Gan BS. Shear-bond behavior of self-compacting geopolymer concrete to conventional concrete. Construction and Building Materials 2022; 321. https://doi.org/10.1016/j.conbuildmat.2021.126167

[61] Purwanto P, Ekaputri JJ, Nuroji N, Indriyantho BR, Gan BS, Han AL. Geopolymer haunch beam–column connection behavior. Arabian Journal for Science and Engineering 2023. https://doi.org/10.1007/s13369-023-07921-7

[62] Xu G, Shi X. Characteristics and applications of fly ash as a sustainable construction material: a state-of-the-

art review. Resources Conservation and Recycling 2018; 136: 95–109. https://doi.org/10.1016/j.r esconrec.2018.04.010

[63] Ahmad MR, Medepalli S, Wang T, Dai JG, Zheng Y, Ishida T. Effect of alkali-hydroxide on hydration kinetics and microstructure of high-volume fly ash blended cement pastes. Cement and Concrete Research 2024; 185. https://doi.org/10.1016/j.cemconres.2024.107641

[64] Aguirre-Guerrero AM, Robayo-Salazar RA, de Gutiérrez RM. A novel geopolymer application: coatings to protect reinforced concrete against corrosion. Applied Clay Science 2017; 135: 437–446. https://doi.org/10.1016/j.clay.2016.10.029

[65] Yang J, Ding Q, Zhang G, Hou D, Zhao M, Cao J. Effect of sulfate attack on the composition and micro-mechanical properties of C-A-S-H gel in cement-slag paste: a combined study of nanoindentation and SEM-EDS. Construction and Building Materials 2022; 345. https://doi.org/10.1016/j.conbuildmat.2022.128275

[66] Ding Q, Yang J, Hou D, Zhang G. Insight on the mechanism of sulfate attacking on the cement paste with granulated blast furnace slag: an experimental and molecular dynamics study. Construction and Building Materials 2018; 169: 601–611. https://doi.org/10.1016/j.conbuildmat.2018.02.148

[67] Gomaa E, Gheni A, ElGawady MA. Repair of ordinary Portland cement concrete using ambient-cured alkali-activated concrete: interfacial behavior. Cement and Concrete Research 2020; 129. https://doi.org/10.1016/j.cemconres.2019.105968

[68] Gupta R, Tomar AS, Mishra D, Sanghi SK. Multifaceted geopolymer coating: material development, characterization and study of long term anti-corrosive properties. Microporous and Mesoporous Materials 2021; 317: 110995. https://doi.org/10.1016/j.micromeso.2021.110995

[69] Van Tuan N, Ye G, Van Breugel K, Copuroglu O. Hydration and microstructure of ultra high performance concrete incorporating rice husk ash. Cement and Concrete Research 2011; 41(11): 1104–1111. https://doi.org/10.1016/j.cemconres.2011.06.009

[70] Giasuddin HM, Sanjayan JG, Ranjith PG. Strength of geopolymer cured in saline water in ambient conditions. Fuel 2013; 107: 34–39. https://doi.org/10.1016/j.fuel.2013.01.035

[71] Juengsuwattananon K, Winnefeld F, Chindaprasirt P, Pimraksa K. Correlation between initial SiO_2/Al_2O_3, Na_2O/Al_2O_3, Na_2O/SiO_2 and H_2O/Na_2O ratios on phase and microstructure of reaction products of metakaolin–rice husk ash geopolymer. Construction and Building Materials 2019; 226: 406–417. https://doi.org/10.1016/j.conbuildmat.2019.07.146

[72] Scrivener KL, Nonat A. Hydration of cementitious materials, present and future. Cement and Concrete Research 2011; 41: 651–665. https://doi.org/10.1016/j.cemconres.2011.03.026

[73] Lian C, Zhuge Y, Beecham S. The relationship between porosity and strength for porous concrete. Construction and Building Materials 2011; 25(11): 4294–4298. https://doi.org/10.1016/j.conbuildmat.2011.05.005

[74] Zhang J, Bian F, Zhang Y, Fang Z, Fu C, Guo J. Effect of pore structures on gas permeability and chloride diffusivity of concrete. Construction and Building Materials 2018; 163: 402–413. https://doi.org/10.1016/j.conbuildmat.2017.12.111

[75] Negahban E, Bagheri A, Sanjayan J. Pore gradation effect on Portland cement and geopolymer concretes. Cement and Concrete Composites 2021; 122: 104141. https://doi.org/10.1016/j.cemconcomp.2021.104141

[76] Amorim Júnior NS, Andrade Neto JS, Santana HA, Cilla MS, Ribeiro DV. Durability and service life analysis of metakaolin-based geopolymer concretes with respect to chloride penetration using chloride migration test and corrosion potential. Construction and Building Materials 2021; 287: 122970. https://doi.org/10.1016/j.conbuildmat.2021.122970

[77] Lee NK, Lee HK. Influence of the slag content on the chloride and sulfuric acid resistances of alkali-activated fly ash/slag paste. Cement and Concrete Composites 2016; 72: 168–179. https://doi.org/10.1016/j.cemconcomp.2016.06.004

[78] Mangat PS, Ojedokun OO. Free and bound chloride relationships affecting reinforcement cover in alkali activated concrete. Cement and Concrete Composites 2020; 112: 103692. https://doi.org/10.1016/j.cemconcomp.2020.103692

[79] Gunasekara C, Law D, Bhuiyan S, Setunge S, Ward L. Chloride induced corrosion in different fly ash based geopolymer concretes. Construction and Building Materials 2019; 200: 502–513. https://doi.org/10.1016/j.conbuildmat.2018.12.168

[80] Cai W, Xu Z, Zhang Z, Hu J, Huang H, Ma Y, Zhang Z, Wang H, Yin S, Wei J, Shi C, Yu Q. Chloride binding behavior of synthesized reaction products in alkali-activated slag. Composites Part B: Engineering 2022; 238: 109919. https://doi.org/10.1016/j.compositesb.2022.109919

[81] Wang X, Kong L, Zhao W, Liu Y. Chloride transport resistance of alkali-activated concrete exposed to combined chloride, sulfate and carbonation environment. Construction and Building Materials 2023; 367: 130353. https://doi.org/10.1016/j.conbuildmat.2023.130353

[82] Cheng S, Wu Z, Wu Q, Chen X, Shui Z, Lu JX. Degradation characteristics of Portland cement mortar incorporating supplementary cementitious materials under multi-ions attacks and drying-wetting cycles. Journal of Cleaner Production 2022; 363: 132378. https://doi.org/10.1016/j.jclepro.2022.132378

[83] Yu L, Chu H, Zhu Z, Jiang L, Dong H. Determination of the chloride ion content in concrete under simultaneous chloride and sulphate ion attack. Journal of Building Engineering 2023; 72: 106579. https://doi.org/10.1016/j.jobe.2023.106579
[84] Li N, Unluer C. Enhancement of the wet carbonation of artificial recycled concrete aggregates in seawater. Cement and Concrete Research 2024; 175: 107387. https://doi.org/10.1016/j.cemconres.2023.107387
[85] Tran TQ, Cook R, Ipindola O, Fanijo EO, Newman A, Stutzman PE, Brand AS. Measuring mineralized carbon in carbonate minerals and cementitious materials by an acid digestion–titration method. Cement and Concrete Research 2025; 191: 107829. https://doi.org/10.1016/j.cemconres.2025.107829
[86] Kurihara R, Cheng L, Igami R, Wang Z, Aili A, Noto K, Tanaka M, Takahashi H, Maruyama I. Application of acid digestion-based total inorganic carbon measurement for carbonated cement-based materials. Journal of CO2 Utilization 2025; 102: 103266. https://doi.org/10.1016/j.jcou.2025.103266
[87] Kamennaya NA, Ajo-Franklin CM, Northen T, Jansson C. Cyanobacteria as biocatalysts for carbonate mineralization. Minerals 2012; 2: 338–364. https://doi.org/10.3390/min2040338
[88] De Muynck W, Ramirez AM, De Belie N, Verstraete W. Evaluation of strategies to prevent algal fouling on white architectural and cellular concrete. International Biodeterioration and Biodegradation 2009; 63(6): 679–689. https://doi.org/10.1016/j.ibiod.2009.04.007
[89] Sun X, Wai OWH, Xie J, Li X. Biomineralization to prevent microbially induced corrosion on concrete for sustainable marine infrastructure. Environmental Science and Technology 2024; 58(1): 522–533. https://doi.org/10.1021/acs.est.3c04680
[90] Zhang Y, Li T, Hou D, Zhang J, Jiang J. Insights on magnesium and sulfate ions' adsorption on the surface of sodium alumino-silicate hydrate (NASH) gel: a molecular dynamics study. Physical Chemistry Chemical Physics 2018; 20(27): 18297–18310. https://doi.org/10.1039/C8CP02469C
[91] Seo J, Kim N, Yang B, Kim GM. Alterations in the reaction properties of Portland cement against coupled deteriorations of magnesium and sulfate upon carbonation curing. Construction and Building Materials 2023; 400: 132806. https://doi.org/10.1016/j.conbuildmat.2023.132806
[92] Gunjal SM, Turkane SD, Patankar SV, Kondraivendhan B. Effect of magnesium sulphate and sulphuric acid attack on limestone calcined clay cement concrete. Materials Today: Proceedings 2023. https://doi.org/10.1016/j.matpr.2023.03.488
[93] El-Khoury M, Roziere E, Grondin F, Cortas R, Chehade FH. Experimental evaluation of the effect of cement type and seawater salinity on concrete offshore structures. Construction and Building Materials 2022; 322: 126471. https://doi.org/10.1016/j.conbuildmat.2022.126471
[94] Neumann A, Klinkenberg M, Curtius H. Analysis of the secondary phases formed by corrosion of U3Si2-Al research reactor fuel elements in the presence of chloride rich brines. Materials 2018; 11(7). https://doi.org/10.3390/ma11071121
[95] Martin C, Manu E, Hou P, Adu-Amankwah S. Circular economy, data analytics, and low carbon concreting: a case for managing recycled powder from end-of-life concrete. Resources, Conservation and Recycling 2023; 198: 107197. https://doi.org/10.1016/j.resconrec.2023.107197
[96] Liu S, Liu Z, Harada K, Takasu K, Suyama H, Yamamoto H. Investigating the use of bamboo charcoal to reduce carbon emissions in geopolymer mortar. Construction and Building Materials 2024; 434: 136781. https://doi.org/10.1016/j.conbuildmat.2024.136781
[97] Sandanayake M, Gunasekara C, Law D, Zhang G, Setunge S. Greenhouse gas emissions of different fly ash based geopolymer concretes in building construction. Journal of Cleaner Production 2018; 204: 399–408. https://doi.org/10.1016/j.jclepro.2018.08.311
[98] Thannimalay L, Yusoff S, Zawawi NZ. Life cycle assessment of sodium hydroxide. Australian Journal of Basic and Applied Sciences 2013; 7(2): 421–431.
[99] Shi Y, Long G, Ma C, Xie Y, He J. Design and preparation of ultra-high performance concrete with low environmental impact. Journal of Cleaner Production 2019; 214: 633–643. https://doi.org/10.1016/j.jclepro.2018.12.318
[100] Turner LK, Collins FG. Carbon dioxide equivalent (CO2-e) emissions: a comparison between geopolymer and OPC cement concrete. Construction and Building Materials 2013; 43: 125–130. https://doi.org/10.1016/j.conbuildmat.2013.01.023
[101] Fernando S, Gunasekara C, Law DW, Nasvi MCM, Setunge S, Dissanayake R. Life cycle assessment and cost analysis of fly ash–rice husk ash blended alkali-activated concrete. Journal of Environmental Management 2021; 295: 113140. https://doi.org/10.1016/j.jenvman.2021.113140
[102] Alnahhal MF, Alengaram UJ, Jumaat MZ, Abutaha F, Alqedra MA, Nayaka RR. Assessment on engineering properties and CO2 emissions of recycled aggregate concrete incorporating waste products as supplements to Portland cement. Journal of Cleaner Production 2018; 203: 822–835. https://doi.org/10.1016/j.jclepro.2018.08.292
[103] Collins F. Inclusion of carbonation during the life cycle of built and recycled concrete: influence on their carbon footprint. International Journal of Life Cycle Assessment 2010; 15(6): 549–556. https://doi.org/10.1007/s11367-010-0191-4

[104] Sun Y, Cai J, Xu L, Ma X, Pan J. Mechanical and environmental performance of engineered geopolymer composites incorporating ternary solid waste. Journal of Cleaner Production 2024; 441: 141065. https://doi.org/10.1016/j.jclepro.2024.141065
[105] Flower DJM, Sanjayan JG. Greenhouse gas emissions due to concrete manufacture. International Journal of Life Cycle Assessment 2007; 12(5): 282–288. https://doi.org/10.1065/lca2007.05.327
[106] Zhao J, Wang A, Zhu YC, Dai JG, Xu Q, Liu K, Hao F, Sun D. Manufacturing ultra-high performance geopolymer concrete (UHPGC) with activated coal gangue for both binder and aggregate. Composites Part B: Engineering 2024; 284: 111723. https://doi.org/10.1016/j.compositesb.2024.111723
[107] Botto S. Tap water vs. bottled water in a footprint integrated approach. Nature Precedings 2009. https://doi.org/10.1038/npre.2009.3407.1
[108] Zhang X, Wu Z, Xie J, Hu X, Shi C. Trends toward lower-carbon ultra-high performance concrete (UHPC) – a review. Construction and Building Materials 2024; 420: 135602. https://doi.org/10.1016/j.conbuildmat.2024.135602
[109] Li G, Zhang W, Li J, Jiang Y, Zhang Y. Effect of sewage sludge ash on high-temperature resistance, carbon emissions and economic performance of eco-friendly geopolymer mortar. Case Studies in Construction Materials 2025; 23: e05424. https://doi.org/10.1016/j.cscm.2025.e05424
[110] Thannimalay L, Yusoff S, Zawawi NZ. Life cycle assessment of sodium hydroxide. Australian Journal of Basic and Applied Sciences 2013; 7(2): 421–431.
[111] McLellan BC, Williams RP, Lay J, Van Riessen A, Corder GD. Costs and carbon emissions for geopolymer pastes in comparison to ordinary Portland cement. Journal of Cleaner Production 2011; 19(9–10): 1080–1090. https://doi.org/10.1016/j.jclepro.2011.02.010
[112] Song Y, Tian Y, Li X, Wei J, Zhang H, Bond PL, Yuan Z, Jiang G. Distinct microbially induced concrete corrosion at the tidal region of reinforced concrete sewers. Water Research 2019; 150: 392–402. https://doi.org/10.1016/j.watres.2018.11.083
[113] Tian Y, Bao J, Guo W, Zhang P, Cui Y, Zhao T. Autogenous self-healing of cracked concrete exposed to the marine tidal zone. Construction and Building Materials 2022; 357: 129336. https://doi.org/10.1016/j.conbuildmat.2022.129336
[114] Khan MBE, Shen L, Dias-da-Costa D. Self-healing behaviour of bio-concrete in submerged and tidal marine environments. Construction and Building Materials 2021; 277: 122332. ttps://doi.org/10.1016/j.conhbuildmat.2021.122332
[115] Cao J, Peng H, Zhang B, Yang Z, Pan H, Chen J, Zhao X. Basalt fiber-reinforced seawater sea-sand geopolymer composites for offshore engineering constructions: mechanical performance, microstructure, enhanced mechanisms and sustainability. Construction and Building Materials 2025; 493: 143129. https://doi.org/10.1016/j.conbuildmat.2025.143129
[116] Harilal M, Anandkumar B, Lahiri BB, George RP, Philip J, Albert SK. Enhanced biodeterioration and biofouling resistance of nanoparticles and inhibitor admixed fly ash based concrete in marine environments. International Biodeterioration and Biodegradation 2020; 155: 105088. https://doi.org/10.1016/j.ibiod.2020.105088
[117] Ekaputri JJ, Budiman AD, Prawira NN, Sutikno RG, Ahmad FA, Mahendra YFI, Saputra AAI, Gunawan A, Wibowo YG, Petrus HTBM, Wirahadikusumah RD, Sjah J, Katili I, Kusbiantoro A. Dual-function valorization of low-grade fly ash via zeolitization for environmental remediation and concrete enhancemen. Green Technologies and Sustainability 2026; 4: 100426. https://doi.org/10.1016/j.grets.2026.100426